DEMONSTRATION OF CLEAN PARTICLE SEEDING FOR PARTICLE IMAGE VELOCIMETRY IN A CLOSED CIRCUIT SUPERSONIC WIND TUNNEL

Charles M. McNiel, First Lieutenant, USAF

AFIT/GAE/ENY/07-M19

DEPARTMENT OF THE AIR FORCE
AIR UNIVERSITY

AIR FORCE INSTITUTE OF TECHNOLOGY

Wright-Patterson Air Force Base, Ohio

The views expressed in this thesis are those of the author and do not reflect the official policy or position of the United States Air Force, Department of Defense, or the U.S. Government.

AFIT/GAE/ENY/07-M19

DEMONSTRATION OF CLEAN PARTICLE SEEDING FOR PARTICLE IMAGE VELOCIMETRY IN A CLOSED CIRCUIT SUPERSONIC WIND TUNNEL

THESIS

Presented to the Faculty

Department of Aeronautical Engineering

Graduate School of Engineering and Management

Air Force Institute of Technology

Air University

Air Education and Training Command

In Partial Fulfillment of the Requirements for the

Degree of Master of Science in Aeronautical Engineering

Charles M. McNiel, BS

First Lieutenant, USAF

March 2007

AFIT/GAE/ENY/07-M19

DEMONSTRATION OF CLEAN PARTICLE SEEDING FOR PARTICLE IMAGE VELOCIMETRY IN A CLOSED CIRCUIT SUPERSONIC WIND TUNNEL

Charles M. McNiel, BS

First Lieutenant, USAF

Approved:

_____//signed//_____	_____
Dr. Mark F. Reeder (Chairman)	Date
_____//signed//_____	_____
Dr. Paul I. King (Member)	Date
_____//signed//_____	_____
Lt Col Raymond C. Maple (Member)	Date

AFIT/GAE/ENY/07-M19

Abstract

The purpose of this research was to determine whether solid carbon dioxide (CO_2) particles might provide a satisfactory, and cleaner, alternative to traditional seed material for Particle Image Velocimetry (PIV) for use in a closed circuit supersonic wind tunnel. The Air Force Institute of Technology (AFIT) closed circuit pressure-vacuum supersonic wind tunnel was utilized, which achieves a nominal Mach number of Mach 2.9 in a 2.5 inch by 2.5 inch square test section. CO_2 was dispensed into the flow as a liquid from a standard compressed gas liquid tank through two different injector styles at two injection sites using various injector attitudes. Upon exiting the injector in either the stagnation chamber or converging-diverging nozzle, the liquid CO_2 rapidly formed solid particles which became entrained in the wind tunnel flow and began the sublimation process from a solid to a gaseous state. The particles traveled through the test section, in which they were illuminated by a laser, and the light scattered by the particles was imaged with a camera. The resulting images were processed using the Dantec Dynamics FlowManager PIV processing software to generate vector maps representing the flow field in the test section. The particles fully sublimated after traveling through the test section, making the injection process self cleaning and hazard free. Vector maps that matched the nominal 606 m/s velocity in the empty test section were generated utilizing both multi-port tube and shroud tube style injectors. Realistic vector maps were also generated for the flow with a 10˚ half-angle cone model placed inside the test section. Overall this research successfully demonstrated the use of CO_2 as a seed material for PIV processing.

Acknowledgments

I would like to express sincere gratitude to my faculty advisor, Dr. Mark Reeder, for the guidance and support that he gave me throughout this project. In addition, I thank John Hixenbaugh of the Air Force Institute of Technology for the technical and operational assistance he gave me. I would also like to thank Innovative Scientific Solutions, Inc. and Dantec Dynamics for the invaluable technical assistance they provided. I also owe thanks to my thesis sponsor of the Air Force Research Lab, Air Vehicles Directorate. Finally, I owe gratitude to my loving wife for her support and encouragement throughout the duration of my work on this thesis.

Charles M. McNiel

Table of Contents

Page

List of Figures

Page

List of Tables

Page

DEMONSTRATION OF CLEAN PARTICLE SEEDING FOR PARTICLE IMAGE VELOCIMETRY IN A CLOSED CIRCUIT SUPERSONIC WIND TUNNEL

I. Introduction

Section 1 - Motivation

In traditional wind tunnel experiments, most measurement techniques involve the use of intrusive elements inside the test section. Forces and moments are measured by a balance, and velocity information is gathered using a probe inserted in the flow. These techniques can provide useful information, but they unquestionably affect the flow and, to varying degrees, the measurements that they are making. With the advent of powerful computational fluid dynamics (CFD) modeling, both simple and complex flow regimes can be simulated, providing useful data and information to aerodynamicists. However, even the best CFD models cannot substitute for empirical data in some cases, and wind tunnel experimentation has proven its continuing value time and time again.

Within the past 15 years a new technique called Particle Image Velocimetry, or PIV, has been developed to address the problem of intrusiveness with traditional wind tunnel velocity measurement systems. In this method, the wind tunnel flow is seeded with tracer particles that disperse and track the motion of the fluid. If the particles are of suitable size, they will accurately follow the flow and can be considered representative elements of the fluid. In PIV these seed particles are illuminated by a light source, usually a laser sheet, and the light scattered by the particles is collected by a camera. In this fashion, two images are captured in very rapid succession, and the resulting images can be correlated using the known time interval between image captures and the distance

traveled by the particles to calculate two components of representative velocity vectors for each particle. These velocity vectors, when taken across the entire image area, provide a velocity vector map that represents the flow within the illumination plane.

Determining which seed particle to use for PIV is very important. The seed particles must be large enough to scatter sufficient light for imaging, but small enough to accurately track the fluid flow. In addition, the number of particles in the seeding volume must be addressed so that the spatial resolution of particles provides images suitable for processing. Traditionally, materials used for particle seeding in gas flow PIV have included solids like polystyrene, aluminum oxide, titanium dioxide, dioctylphathalate and magnesium oxide. Atomized liquids like glycol, water and silicone oil have also been commonly used (13:19).

These traditional PIV seed materials, while physically suitable for gas flows, coat the walls and surfaces inside the wind tunnels and can also present fire or combustion hazards in some cases. Using them has proven effective for open circuit wind tunnels, since the particles are ejected from the wind tunnel with the flow, making clean-up and maintenance minimal. But in closed circuit tunnels, in which the flow is recirculated through the tunnel system, traditional PIV seeding materials pose serious problems. These problems include costly clean-up efforts, lengthy wind tunnel down-time, potentially hazardous environments and damage to wind tunnel components and expensive models.

When solid particles are introduced into high speed gas flows, they can damage compressor blades, flow driers, flow straighteners and flow turning elements. Liquid

seeding particles can coat all surfaces inside a tunnel and create a tedious clean-up situation. Water based liquid particles can also impart undue corrosion to wind tunnel elements, reducing their life and operating effectiveness. Models in the wind tunnel can also suffer adverse effects from the use of traditional solid or liquid seeding materials. Pressure sensitive paint applied to aerodynamic surfaces can be damaged when liquid particles come into contact with the model.

In addition to these concerns, other potentially dangerous situations can be created for wind tunnel operators. Particles are easily inhaled by personnel, and if the material is hazardous then serious health problems can arise. Also, traditional PIV materials such as aluminum oxide can be flammable, and if the right concentrations are present, fires and/or explosions can result (17:169).

As a result of these complications and dangers, many large-scale closed circuit wind tunnel facilities in the Department of Defense and NASA have chosen not to pursue the inclusion of PIV among their test capabilities (2). The use of a non-intrusive seeding material could potentially solve the problems that traditional materials present to the use of PIV in closed circuit tunnels. Ideally, a seeding material will accurately track the flow, sufficiently scatter light, be self-cleaning, not damage or coat wind tunnel components or models and present no health hazards or combustion dangers. This research thesis focuses on the use of one such candidate seeding material for PIV, solid carbon dioxide (CO_2).

For PIV seeding, CO_2 is introduced into the wind tunnel from a compressed tank with a siphon drawing liquid CO_2 through an injector. As the CO_2 exits the injector, the

pressure and temperature reduction from the tank to the wind tunnel causes the liquid CO_2 particles to transition into the solid state. The solid particles then track the flow through the test section, in which they are illuminated by the laser. In the solid state the particles continue to change phase, from solid to gaseous through the process of sublimation. This seeding process is self-cleaning, and provides ample particles suitable for PIV. Since the CO_2 particles begin to undergo sublimation as soon as they are introduced to the free stream, they must be of sufficient size to persist through the test section. On the other hand, they must be small enough to accurately follow the flow field.

The research presented in the following sections includes a summary of traditional PIV techniques and seeding materials. Additionally, experimental data will be provided showing the successful velocity measurement of CO_2 particle seeding in a closed circuit supersonic wind tunnel using a commercially available Dantec Dynamics PIV system.

Section 2 - Overview of Test Equipment

This research involved the use of a closed circuit pressure-vacuum supersonic wind tunnel, illustrated in Figure 1. Pressurized air, stored at approximately 190 psig, is fed into a stilling chamber through a pressure reducing control valve, which sets the pressure in the chamber at approximately 25 psig. The air then enters a converging-diverging nozzle which accelerates the flow to Mach 2.9 in the 2.5 inch by 2.5 inch test section. The supersonic air is then evacuated from the tunnel into a vacuum chamber.

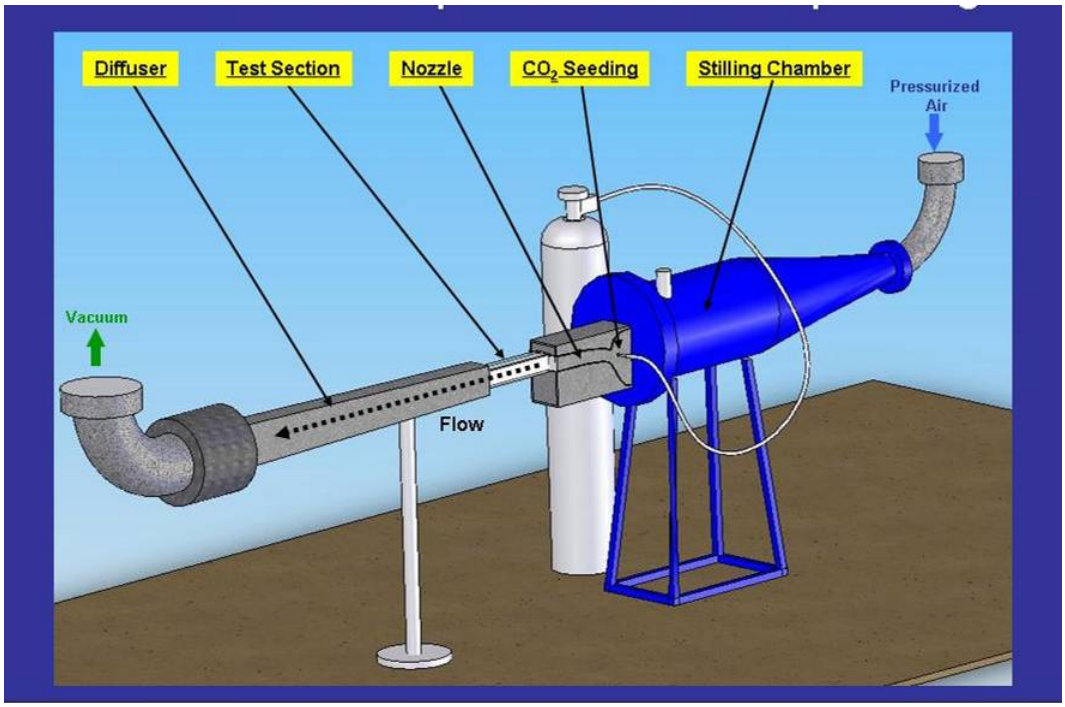

Figure 1: Wind tunnel experimental setup

A significant portion of this research was devoted to determining the proper design, location and orientation for an injector to create particle seeding that is most suitable for PIV processing. As illustrated in Figure 1, liquid CO_2 was initially injected

into the nozzle sidewall. CO_2 injection was also accomplished via the top of the stilling chamber to investigate the suitability of alternative injection sites. Two different injectors were designed and used in this research, which will be described in detail in Chapter three.

A Dantec Dynamics© FlowMap PIV system was utilized to perform illumination, imaging, processing and storage functions in this research. This system is one of a number of commercially available PIV systems. As shown in Figure 2, the camera is a Redlake Megaplus ES Model 4.0/E high speed monochromatic camera with an 80mm Nikon lens. The particles are illuminated with a New Wave Research Solo 120 yttrium aluminum garnet (YAG) laser shown in Figure 3, which contains two separate frequency-doubled lasers that emit light at a wavelength of 532 μm, allowing precise time separation of two pulses. The PIV system is controlled with the Dantec FlowMap System Hub controller, and the images are processed on a desktop computer using Dantec's FlowManager software, as seen in Figure 4.

Figure 2: Redlake Megaplus ES 4.0/E camera

Figure 3: New Wave Research Solo 120 YAG laser

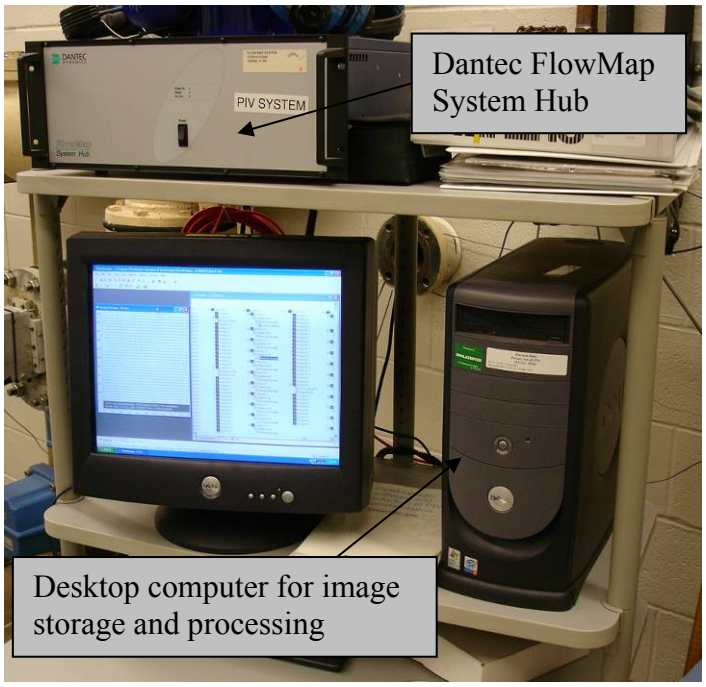

Figure 4: Dantec PIV system components

Section 3 - Research Focus and Goals

The focus of this research is to demonstrate the use of CO_2 as the seeding material for flow field velocity computations using a commercially available PIV system. For the completion of this task, the following steps were taken:

- Demonstrate ability to generate CO_2 particles and capture images using an empty wind tunnel test section
- Investigate particle size, quantity and homogeneity in an empty wind tunnel resulting from the use of:
    - Two different injector sites
    - Two different injector designs

    - Multiple injector attitudes with respect to flow direction at each injection site
- Determine procedure for processing images to obtain vector maps that most accurately represent the known velocity in the wind tunnel

Further discussion of the importance of each of these tasks follows.

Generation of particles and capture of images using CO_2 seeding

Preparing the experimental setup for the preliminary demonstration of CO_2 seeding and PIV imaging was the first step taken in this research effort. When this project began the closed circuit supersonic wind tunnel used in this effort had not been active for approximately two months while modifications to the air supply system were made, and a few critical components in the actuation and control system for the tunnel had been upgraded to a National Instruments system. The system was brought online and a few dry runs were performed to ensure the tunnel would be operating normally. After that, the camera and laser were positioned and aligned to ensure the images captured by the PIV system would be usable. Finally, the multi-port injector was fitted to the liquid CO_2 tank and mounted in the tunnel sidewall. After these preparations had been made, the tunnel was operated with CO_2 introduced using a manual valve which allowed CO_2 to pass through the injector, and images were collected.

Investigation of Various Injection Locations and Attitudes for Two Injectors

In order to obtain suitable particle sizes and distributions required for PIV, as mentioned above, various injector attitudes with respect to the flow direction at two injections sites were investigated using both injector designs. The first injection site tested was the nozzle sidewall; the other site was the top of the stagnation chamber. At each location, the injectors were tested while injecting in the direction of the flow, at 90º transverse to the flow direction, and fully opposed to the flow. Both the multi-port injector and the shroud injector were tested at each location in each direction to observe particle size and distribution, and the images from each individual test run were analyzed with the PIV software to assess their suitability for processing.

Development of Technique for the Generation of Vector Maps

Varying any one of the experimental parameters for a PIV run changed the quality of the images produced. The first step for each unique test run was determining the proper laser sheet thickness, laser distance from the tunnel, camera settings and so forth to generate images suitable for PIV. Once images were reliably captured, they were analyzed using the Dantec FlowManager software to generate representative velocity maps of the flow field. The FlowManager software includes many features and functions that allow it to analyze images with very different particle size and distribution characteristics. Thus, the most effective procedure for generating vector maps is potentially different for each set of experimental parameters. Therefore, various unique

PIV runs were analyzed with the software using different methods to find the procedure that generated vector maps best modeling the known flow field in the test section.

II. Literature Review

Section 1 - Chapter Overview

This chapter summarizes the basics of PIV as well as the history and current state of the art in PIV techniques. Prior research describing the use and characteristics of traditional seeding materials in PIV will also be presented. Additionally, research showing the suitability of CO_2 as the seed material for PIV is discussed.

A thorough study of past and current PIV techniques indicate that the use of CO_2 as a seed material has not been recorded, but CO_2 has been shown to be a viable seeding material in flow visualization tests. The Air Force Research Lab, in conjunction with Princeton University, injected CO_2 into supersonic gas flows and performed Rayleigh scattering (15). In addition, many experiments in subsonic open circuit wind tunnels have used solid CO_2 to condense water droplets for flow visualization and ablation (11).

Section 2 – PIV Basics

The origins of PIV can be traced to the experiments of Ludwig Prandtl, in which particles were suspended in a water tunnel for the visualization of motion around objects (26:2). This was a rudimentary process for qualitative flow visualization, but the principle of seeding a fluid flow for the purpose of extracting useful data lives on today. With current imaging technology and computing power, Prandtl's innovation has been advanced to the point where tiny particles moving at supersonic velocities can be imaged to provide extremely accurate flow data.

A widely referenced source of foundational PIV information is the textbook by M. Raffel, C. Willert, and J. Kompenhans, *Particle Image Velocimetry, a Practical Guide*

(16). This publication also contains a thorough list of references to further expand on the topic of PIV. A diagram of a traditional PIV experimental setup from this book is shown in Figure 5. A brief summary of the components required for PIV follow.

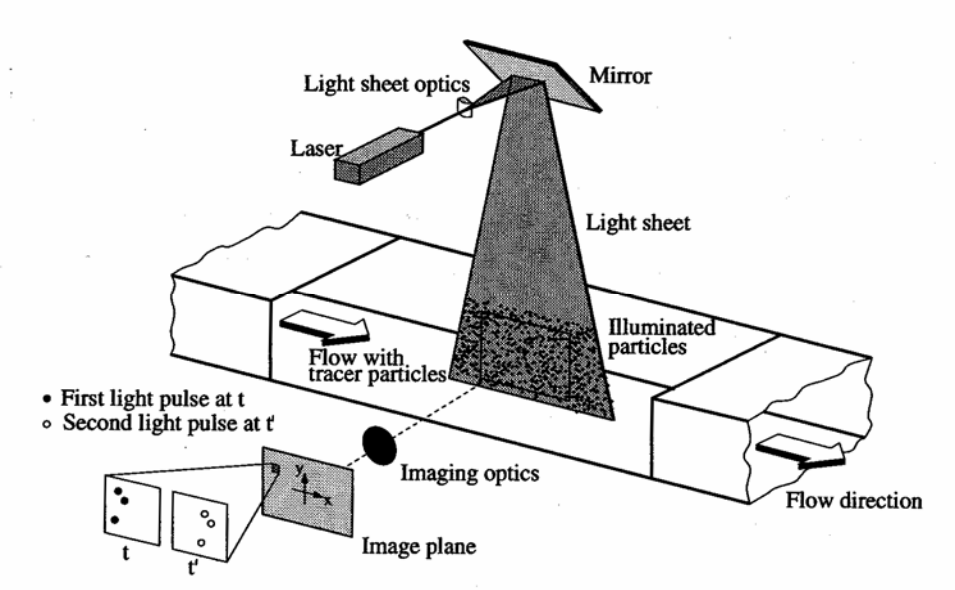

Figure 5: Traditional PIV experimental setup (16:4)

Tracer Particles

Information is extracted from the flow field being studied through the use of tracer particles. The particles are inserted into the flow, and their motion is representative of the motion of the fluid. As such, the particles must be small enough to accurately track the motion of the fluid they are suspended in, but they also must be large enough to scatter enough light for imaging. The illumination of the tracer particles is typically done using a pulsed laser sheet, with the subsequent scattered light captured in images and stored for processing. Only when suitable particles are used will their motion be truly

representative of the flow field. Thus, selection of an appropriate seed material is critical to the generation of accurate velocity vector maps and other data (16).

Illumination Source

Once the flow is seeded with suitable tracer particles, they must be illuminated in order to capture images. Generally, lasers are used for PIV because of their generation of monochromatic light with high intensities. This laser light is easily formed into sheets using optical equipment, which is conducive to lighting a two dimensional plane in space. Many such lasers are used for PIV, including: Copper vapor, Argon ion, Helium-Neon, Yttrium Aluminum Garnet (YAG) and Neodymium doped Yttrium Aluminum Garnet (Nd:YAG) lasers. For the purposes of PIV, pulsed lasers which use Q-switches to suddenly release a high energy pulse are used almost exclusively. Continuous wave lasers, which emit a continuous beam of light at much lower peak power than pulsed lasers, are generally not as common in PIV.

Image Capture

As of late, digital imagers are used exclusively in PIV, but in earlier times film photography was the norm (16:54). The consistency, ease of use, fast image verification and high resolution achieved with digital cameras make them ideal for modern PIV.

This research was conducted using a Redlake Megaplus ES 4.0/E monochromatic camera capable of 2048x2048 pixel resolution. This camera used an 80mm Nikon lens which allowed the field of view to be set at approximately 1.75 inches square from a

focal length of approximately 10 inches. The camera utilizes an electronic shutter than can capture successive images every 0.5 μs.

Image Analysis

Once a set of images is captured, the individual image pairs must be compared computationally to generate velocity data. The notion of determining the velocity of a single particle by measuring its distance traveled, in pixels, over a known time period is simple to understand. However, many factors preclude the use of such a straightforward algorithm in the practice of PIV. The comparison of the signals from two or more images for PIV is called correlation. Traditional auto correlation techniques were reviewed by Adrian (1) and then supplemented by Adrian and Keane (10) with information regarding cross correlation techniques. Original PIV methods employed optical correlation of particles, while modern methods use digital signal processing to correlate images for the generation of velocity vectors (16:117). The Dantec FlowManager image processing system used in this research, like other commercially available systems, utilizes complex adaptive correlation techniques that greatly expand the range and quality of images that can be used to generate useful vector maps (4). The software processing method for generating vector maps is described in detail in Chapter three.

Selecting an appropriate particle seeding material is crucial to successful PIV. The properties of the tracer particles that are most important are: density, size and index of refraction. These properties govern the ability of the tracer particles to follow the flow field accurately and to reflect a sufficient amount of light for quality image capture.

Section 3 – Particle Property Considerations

As a precursor to this research effort, an investigative study was undertaken by Maj Charles J. DeLapp to characterize the properties of solid CO_2 particles for the purposes of PIV (6, 7). In doing so, an extensive search was conducted regarding traditional PIV particle characterization methods. Specifically, the areas of particle motion, particle optical qualities, particle distribution, particle sublimation rate and potential hazards and health impacts were addressed. In addition, traditional PIV seed materials were discussed, with common materials and particle sizes presented (7:26).

III. Methodology

Section 1 – Imaging CO_2 Particles in Supersonic Wind Tunnel

The first step in this research effort was to generate CO_2 particles in the closed circuit supersonic wind tunnel. The initial goal was to simply operate the tunnel and the Dantec PIV system while injecting CO_2 to produce images. The quality of the images and suitability for PIV were not priorities during this initial phase, they were to be considered later.

As mentioned previously, the wind tunnel had not been operated in approximately two months. Key components had been removed from the wind tunnel for repair or replacement, and the blowdown system had not been pressurized or tested since the tunnel was last run. In addition, the Dantec PIV system had not been used to capture particle images in that same period of time. The injector used during the initial CO_2 suitability investigation performed by Maj DeLapp (7) consisted of a single tube of 1/16 inch outside diameter and 0.020 inch inside diameter. The injector to be used in the first phase of this research was the multi-port injector shown in Figure 6. This injector is a 0.19 inch inside diameter closed-end tube with six 0.005 inch CO_2 ejection ports on the side, as shown in Figure 6. A second injector, consisting of a 0.19 inch inside diameter open-ended tube into which a 0.030 inch inside diameter feed tube releases CO_2, was used later in this research effort and is shown in Figure 7. Both injectors were investigated in the nozzle sidewall and stagnation chamber injection sites.

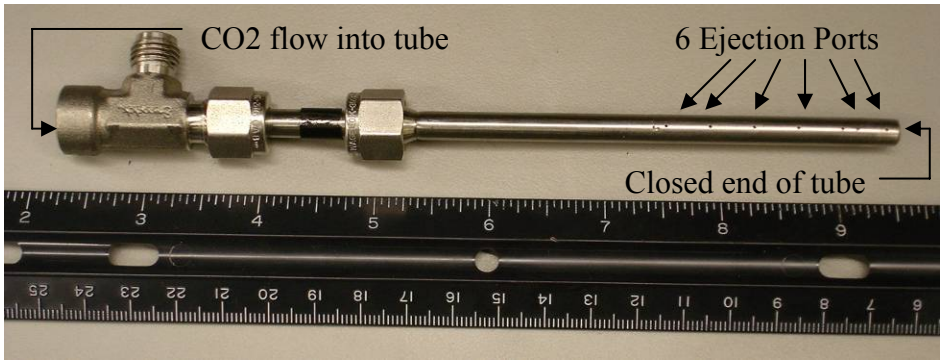

Figure 6: Mult-port CO2 injector

Figure 7: Shroud CO2 injector

The wind tunnel was brought online and the blowdown system was activated to run the tunnel a few times to ensure that the National Instruments LabView control system was causing the pneumatic valves controlling tunnel operation to function properly. The wind tunnel blowdown system consists of two compressors with electronic driers that supply dry air pressurized to 145 psig into a 6,000 gallon tank, as well as a 6,000 gallon vacuum tank that is evacuated by a single vacuum pump. This vacuum assist reduces the pressure required to operate the wind tunnel and allows for run times of approximately 15-20 seconds. Control of the wind tunnel is accomplished using a pressure reducing valve that sets the stilling chamber pressure. All runs for this research were performed with a stagnation pressure of nominally 39 psia, which caused the tunnel to operate at Mach 2.9 at a free stream static pressure of 1.17 psia in the test section. The

test section static temperature was 110 Kelvin and a Reynolds number of $3.9x10^8$ was calculated (9). The wind tunnel setup is shown in Figure 8.

Once successful and safe blowdown was achieved, the injector was placed in the nozzle sidewall and the wind tunnel was operated. The placement and orientation of the injector for these initial runs are shown in Figure 8.

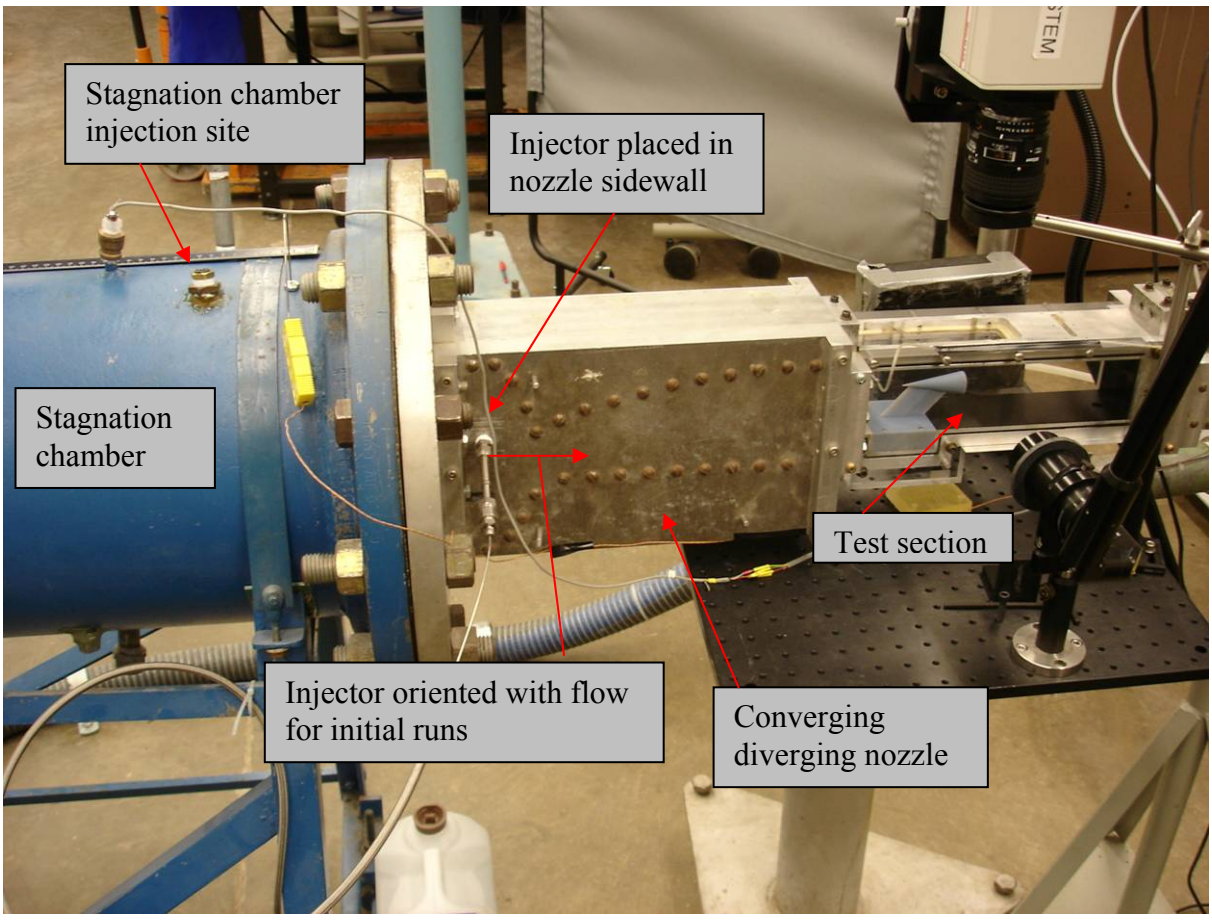

Figure 8: Injection locations for various experimental runs

The PIV system was used to capture a series of images during these initial test runs with the CO_2 injection system operating. These images are shown and discussed in Chapter 4 of this text. An image pair that is highly suitable for PIV processing is shown in Figure 9. An image pair that is well suited for PIV processing has the following traits: particles

that follow the flow accurately, strong light signals from the particles for good contrast and a high signal to noise ratio, an even distribution of particles throughout the area of investigation and sufficient particle density within the area of investigation for good correlation between images.

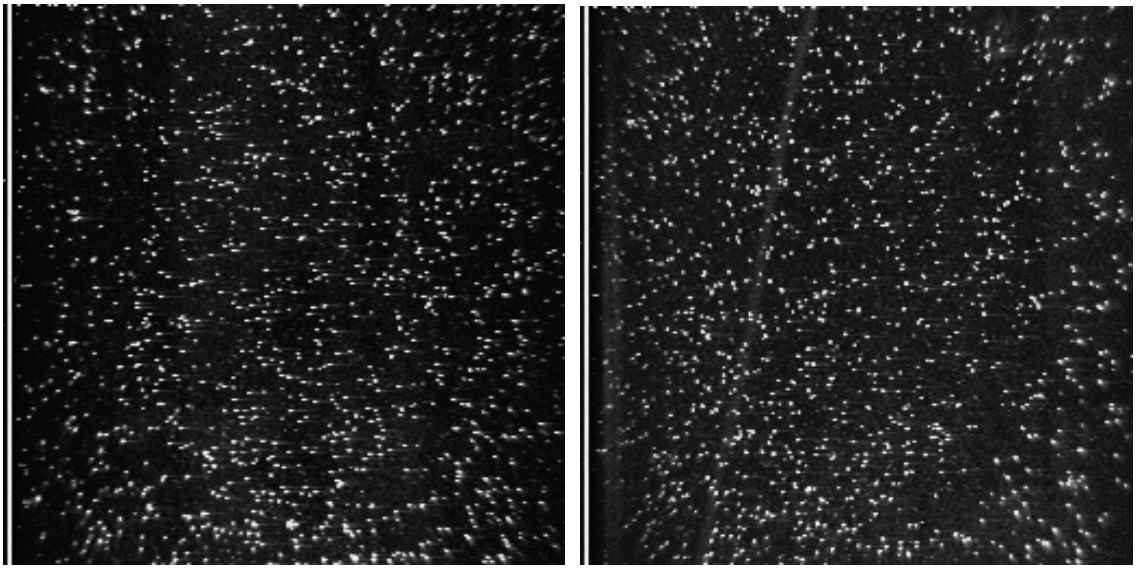

Figure 9: High quality image pair for PIV processing

The Redlake Megaplus ES 4.0/E camera, New Wave Research Solo PIV laser and Dantec laser light arm used for capturing images are all shown in Figure 10. An illustration of the operation of the PIV image capture system is shown in Figure 11.

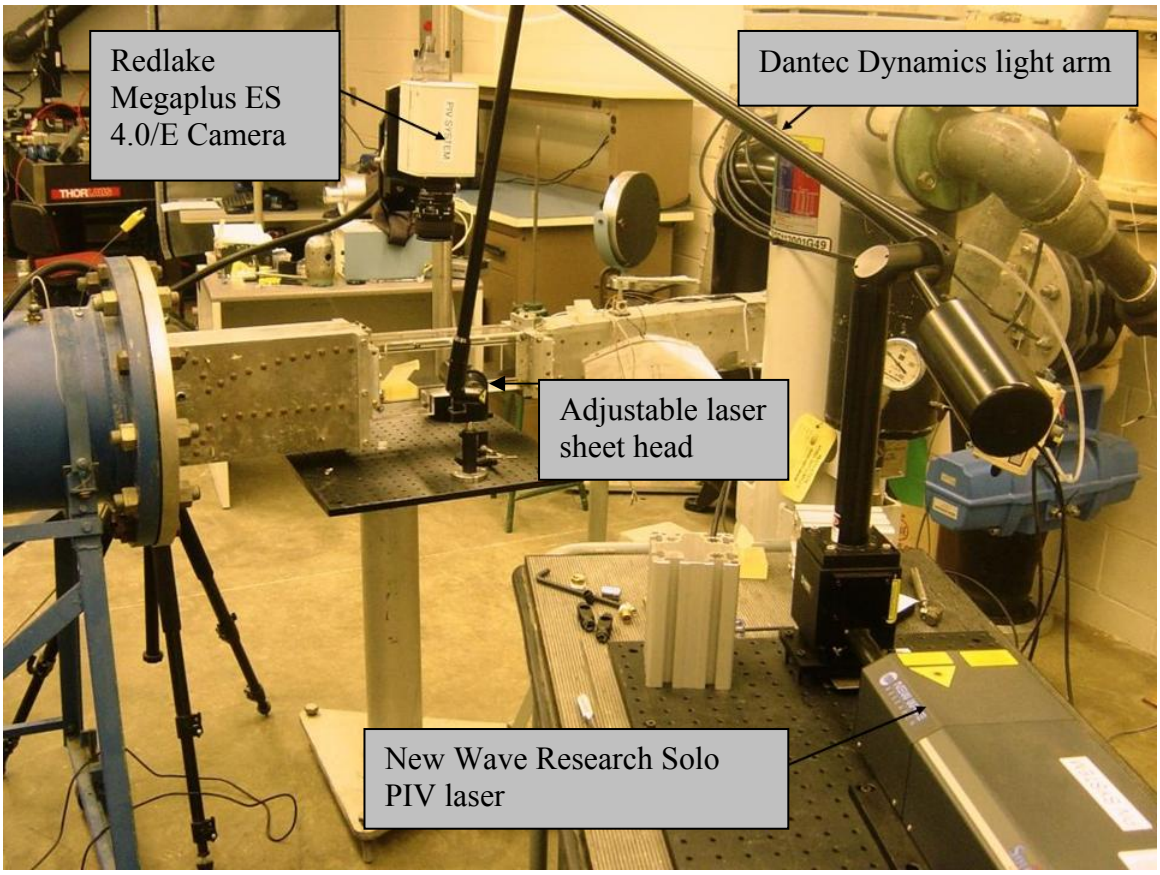

Figure 10: Equipment used for PIV imaging

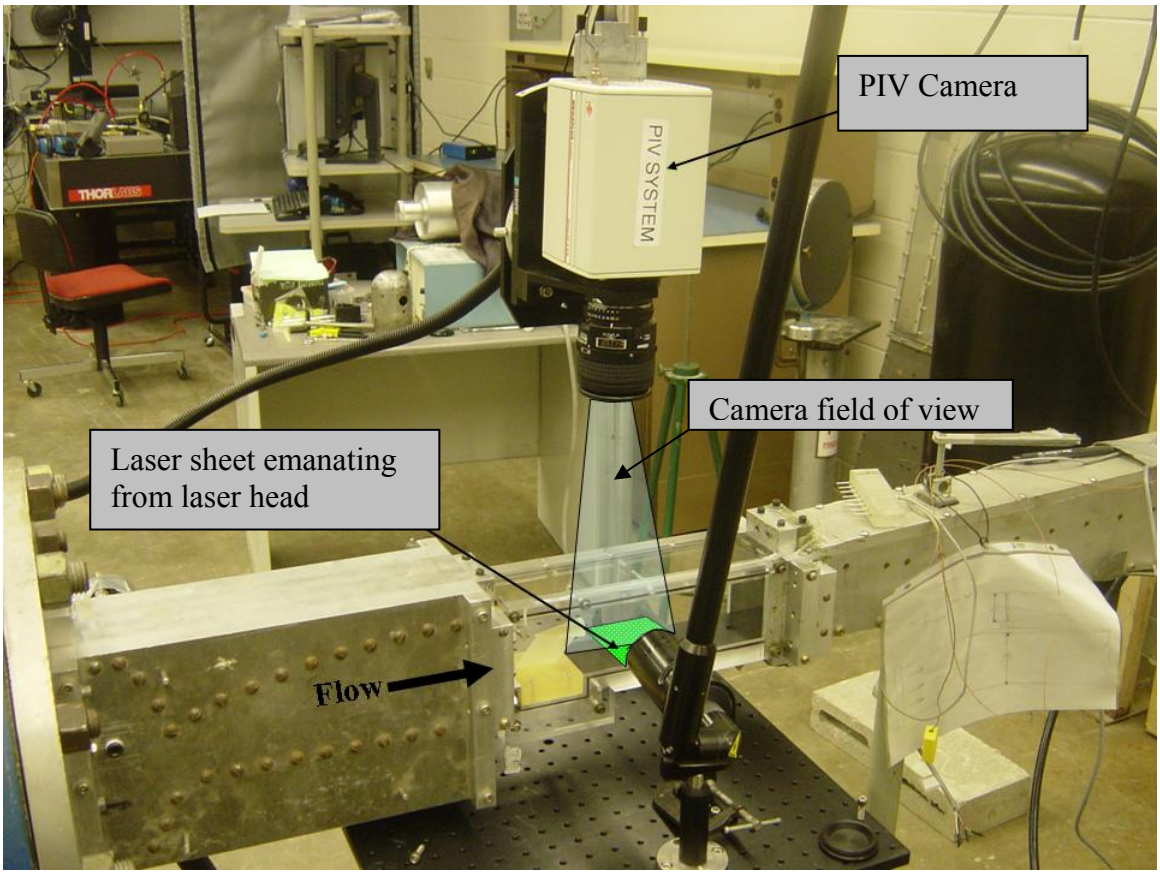

Figure 11: Illustration of PIV image capture system operating (7)

The images were captured according to the image acquisition parameters input to the Dantec FlowMap PIV system hub, which are shown in Table 1. All subsequent PIV runs used these same parameters. Each of the two lasers in the New Wave Research laser illuminated a single image exposure, with the combined first and second exposures and subsequent images constituting an image pair. All image acquisition in this research was performed using the Fixed Time Interval run mode in the FlowManager system. For each run, 50 image pairs were recorded, and image pairs that were collected before or after the period of flow seeding were deleted.

Table 1: Image acquisition parameters

Timing Parameter	Measure (seconds)
Time between first and second laser pulses	1×10^{-6}
Approximate duration of each laser pulse (one pulse per image)	1×10^{-8}
Time between recording of each image pair	5×10^{-1}

Section 2 – Generation of initial Vector Maps

Once the first series of experiments were run using CO_2 as the seeding material, the Dantec FlowManager software package was used to generate a set of initial vector maps from the acquired images. The procedure for generating a vector map, also referred to as an algorithm, is very important. Depending on the quality of the images acquired, different algorithms generate very different results.

Generally speaking, once a PIV image pair was acquired using this setup, a vector map could be produced using the Dantec FlowManager software quickly and easily. There are two correlation methods available in this software to take the light signal information from the images and use that to compute a vector map: auto correlation and cross correlation. Each method uses interrogation areas, which are subsets of the total image, in which the software scans the image for a light signal, represented by a lit particle for PIV. The software then applies Fast Fourier Transforms (FFTs) to the light signals to calculate the average spatial shift of the light sources (particles) to generate velocity data.

Auto correlation uses a single image to generate a vector map. In auto correlation, two successive light pulses expose a single image frame. This method is inferior to cross correlation simply because the software extrapolates particle motion from a single image. This can lead to ambiguity, because of uncertainty relating to whether particles correspond to the first or second illumination. Auto correlation was necessary in early implementations of PIV because camera systems were not able to capture images rapidly enough to generate two separate frames. Many modern cameras are able to generate image pairs reliably and at very high speeds using electronic gating. As such, cross correlation rather than auto correlation was used to generate vector maps in this research effort.

Cross correlation utilizes the FFTs mentioned above to calculate an average spatial shift of particles for each interrogation area. In cross correlation, the total image is divided evenly into a grid of interrogation areas. An example of a 256x256 pixel interrogation area cross correlation grid is shown in Figure 12. With cross correlation, the particle signal for each image is compared to calculate an average spatial shift, and a single displacement vector is generated for each interrogation area.

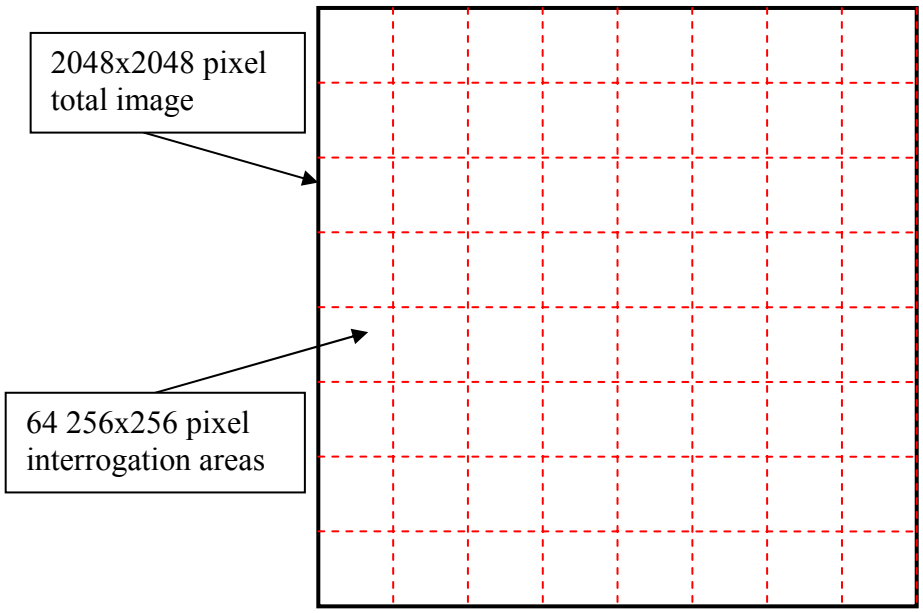

Figure 12: Interrogation area grid for cross correlation of PIV images

Once the scattered light from each particle is collected for each interrogation area for both images in an image pair, the cross correlation technique then compares the signals for each corresponding interrogation area between the two images. An average spatial shift of particles is then calculated, and a representative vector is created for each interrogation area. In cross correlation, the interrogation areas are fixed, and there is no compensation made for particles entering or exiting an interrogation area between the first and second image in an image pair. Thus, a phenomenon known as drop-out can occur, in which a particle escapes the interrogation area between the first and second image of an image pair. This can occur when a particle moves out of the interrogation area parallel to the plane of illumination, or when a particles moves perpendicularly out of plane. To minimize this effect, the time between frames should be adjusted so that the maximum displacement of the seed particles is approximately one-quarter the length of one side of the interrogation area (12).

The linear digital signal processing model for cross correlation that the Dantec FlowManager system utilizes is shown in Figure 13, below.

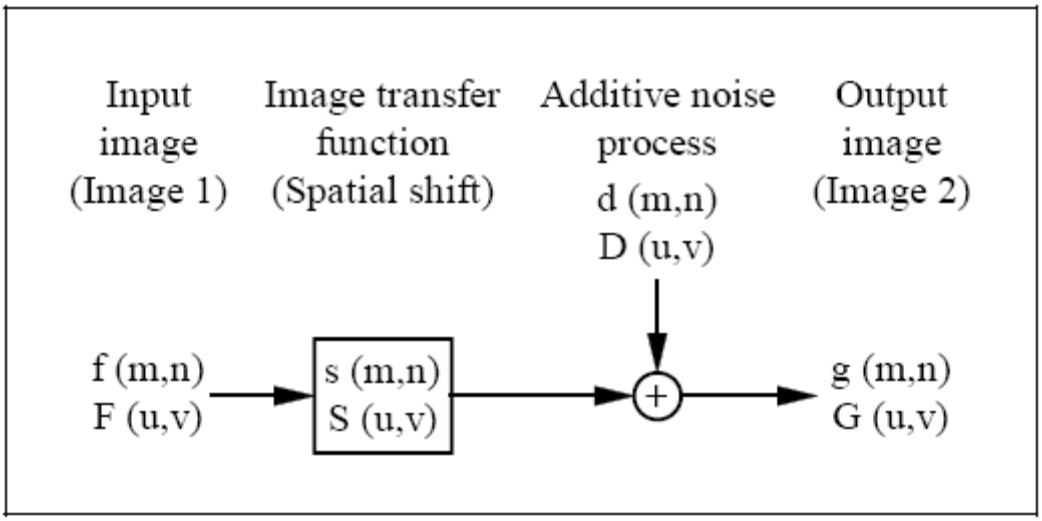

Figure 13: Linear digital signal processing model for PIV cross correlation (5)

The function f (m, n) describes the light intensity within the interrogation area recorded at time t, and the function g (m, n) describes the light intensity recorded at time $t+\Delta t$, where Δt is an incremental length of time. The latter can be considered the output of an image transfer function s (m, n), taking f (m, n) as input, and with the noise function d (m, n) added. Capitalized functions are the Fourier transforms of the corresponding lower case functions, and (u, v) are coordinates in the spatial frequency domain. The spatial shifting function s (m, n) is directly related to the flow and the time between the two recordings, while the noise function d (m, n) is a result of seeding particles moving into or out of the interrogation area in the period between the two recordings, described earlier as drop-out (5).

The major task in PIV is the estimation of the spatial shifting function s (m, n) on the basis of known (measured) values of f (m, n) and g (m, n), but the presence of noise

complicates matters. The method chosen to estimate the displacement function s (m, n) is the statistical technique of spatial cross correlation. The discrete cross correlation function ϕ_{fg} (m, n) of the sampled regions f (m, n) and g (m, n) is given by the expected value:

$$\phi_{fg}(m,n) = E[\, f(m,n), g(m,n)] \qquad \text{(Eq. 1)}$$

where:

$$E[\, f(m,n), g(m,n)] = \sum_{k=-\infty}^{k=\infty} \sum_{l=-\infty}^{l=\infty} f(k,l) \bullet g(k+m, l+n) \qquad \text{(Eq. 2)}$$

In literature, cross correlation values are often normalized to obtain values between 0 and 1, but in this context only relative correlation levels within the investigated interrogation area are of interest (19). A high cross correlation value, or peak, is observed where many particles match up with their corresponding spatially shifted partners; small cross correlation peaks may be observed when individual particles match up with other particles. The former are known as true correlations, while the latter are called random correlations (5).

Seeding particles entering or leaving the interrogation area between the recording of the first and the second image will not contribute to the true correlation since either the initial or final particle position is missing. They do, however, contribute to the random correlations and as such decrease the signal-to-noise ratio. In PIV this phenomenon is often referred to as loss-of-pairs or signal drop-out. Nevertheless, the highest correlation peak can safely be considered to represent the best match between the functions f (m, n) and g (m, n) when the number of matching particle pairs is sufficiently large. The

position of the peak in the correlation plane corresponds directly to the average particle displacement within the interrogation area investigated. In practice, to efficiently compute the correlation plane, Fourier transform processing is used in PIV.

The justification of using FFT processing is as follows: a camera image may be considered a two-dimensional signal field analogous to a one-dimensional time series. Many one-dimensional signal processing techniques can readily be extended to two dimensions, and in this case Fast Fourier Transforms (FFTs) are used to speed up the cross correlation process. Rather than performing a sum over all elements of the sampled region, the operation can be reduced to a complex conjugate multiplication of each corresponding pair of Fourier coefficients. The resulting new coefficients are then inversely transformed to obtain the cross-correlation function, ϕ_{fg}, shown in Equations 1 and 2 (5). The Dantec FlowManager cross correlation process model is illustrated in Figure 14.

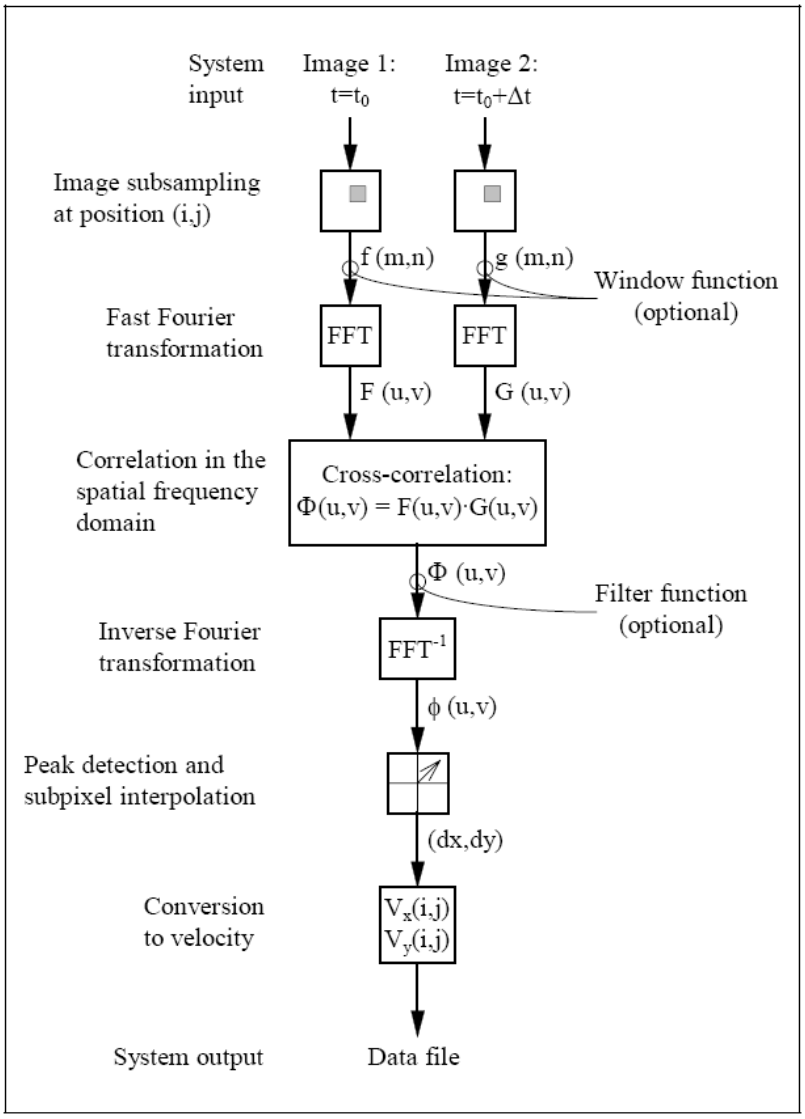

Figure 14: Dantec FlowManager data generation model (5)

A special type of cross correlation is available for use in the Dantec FlowManager software, the adaptive correlation. With this technique, the software generates interrogation areas only where there are particles present. This technique is very useful for circumstances such as those encountered in this research, in which particles do not uniformly fill the entire plane of investigation. For all of the data shown in this thesis, an

adaptive correlation was used to generate vector maps. A further discussion of this technique is included in Chapter four.

Once a set of image pairs has been processed and vector maps have been generated and validated for each image pair, a calculation can be performed to generate a single value-averaged vector map for the entire set. This value-averaged vector map is useful because it generally contains fewer of the spurious vectors that are apparent in the individual image pair vector maps. Each interrogation area for the individual image pair vector maps contributes equally to the averaged vector present in the average vector map.

Section 3 – Refining Injection Technique and System Setup

After the initial vector generation was completed, alternate injector orientations, injection locations and injector types were investigated with the goal of generating images that were most suitable for PIV with the Dantec system.

The multi-port injector shown in Figure 6 was initially placed in the nozzle sidewall and oriented to inject particles in the direction of the flow, as shown in Figure 8. An additional set of runs was accomplished with the injector ports oriented to inject CO_2 opposite to the direction of the flow, and a third set of runs was accomplished with the injector ports oriented transverse, or 90º, to the direction of the flow. All three orientations for the multi-port injector in the nozzle sidewall are shown in Figure 15.

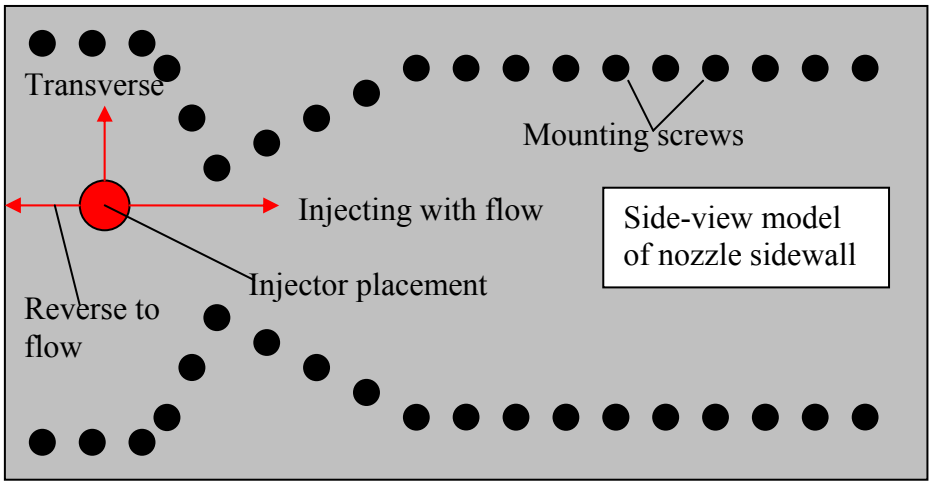

Figure 15: Illustration of injection orientations with multi-port injector

After the different orientations of the multi-port injector were investigated, the injector was moved to the alternate injection site in the stagnation chamber, as shown in Figure 8. Initially, a few experimental runs were made with the multi-port injector oriented to inject CO_2 in the same direction as the flow. Additionally, the injector was turned and CO_2 was injected reverse to the flow.

For the next set of runs, the shroud injector shown in Figure 7 was inserted into the stagnation chamber injection site and a set of runs was accomplished. The injector was set with the tip approximately two inches deep into the cavity of the stagnation chamber. The shroud injector utilized a 0.030 inch inside diameter tube running from the liquid tank's braided steel line to the 0.19 inch inside diameter shroud tube. The 0.030 tube terminated just after entering the shroud tube, and the total shroud tube length is approximately 6.25 inches. In addition, the shroud injector was used in the nozzle sidewall injection location for a set of experiments. The injection depth of the shroud injector was varied over a series of experiments, with deep injection investigated first and

shallow injection investigated second. An end-view of the shroud injector and the two mounting caps used to vary injection depth are shown in Figure 16.

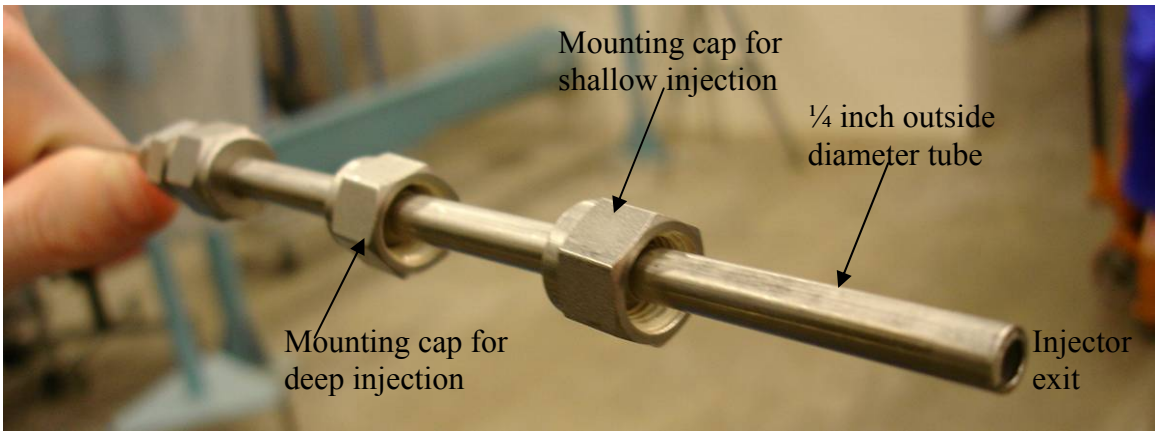

Figure 16: End view of shroud injector

The experiments run with the 10º half-angle cone model in the test section were all accomplished using the shroud injector mounted in the nozzle sidewall. For runs with the cone model present, the injection depth was varied from approximately 2 inches to approximately ¾ inch.

In addition to varying the type of injector, injector locations and orientations and injector depths, different camera and laser settings and orientations were used to generate alternative images for PIV. As a general rule for PIV, the aperture for the camera should be left as open as possible to avoid generating speckle which is similar in appearance to particles and can confuse the vector map generation software (16). Speckle is observed when there is too little light available to the imager in a digital camera, and can be caused by setting the camera aperture too closed. When the aperture is too closed, the reflected light intensity from the particles that reaches the imager is very low. Because of this low light signal, the signal to noise ratio for the light is quite low. The scattering light from each particle interferes with the light from the others, and due to the low signal to noise

ratio, the interference of scattered light on the imager causes speckle (14). The displacement of speckle patterns from particle groups can be used to obtain velocity data, but seeding must be very uniform, and in most cases speckle in a PIV image very closely resembles the particles present in the image. One drawback of setting the aperture open very wide is that the image can suffer washout, in which the light reflected by particles overexposes the image. To address this issue and avoid washout, the laser head was moved further from the tunnel test section to reduce light intensity. Additionally, a Melles Griot 500 nm light filter was placed in front of the camera lens to reduce the amount of 532 nm wavelength laser light that entered the camera lens by 82%. An illustration of the placement of the filter is shown in Figure 17.

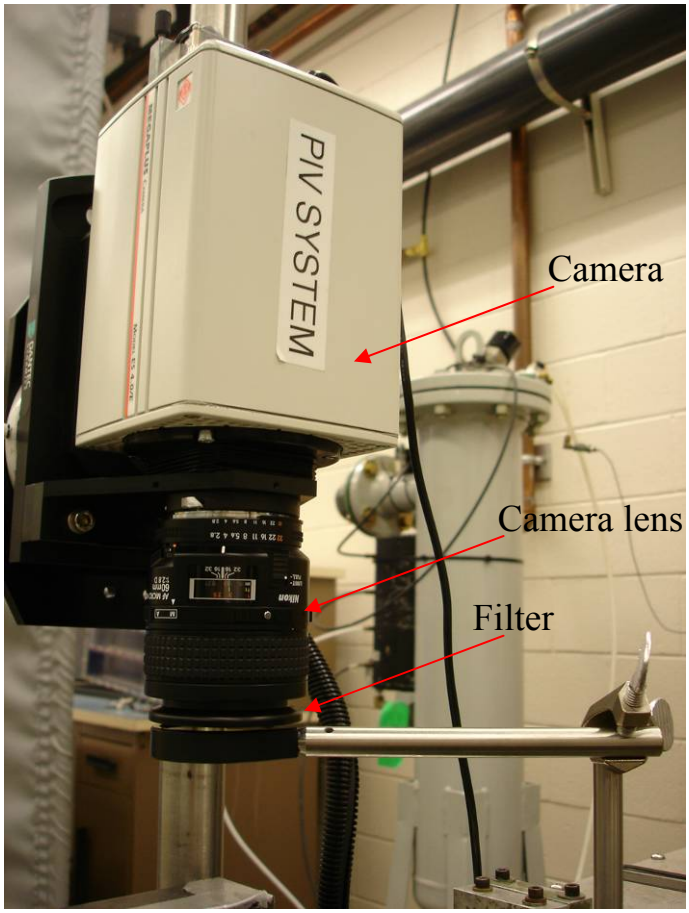

Figure 17: Light filter placed in front of camera lens

Detailed information regarding injector orientations and depths, camera and laser settings and vector map generation algorithms for all of these experimental runs can be found in Chapter four.

Section 4 – Refining the Vector Map Generation Algorithm

Determining the algorithm that produced the most accurate representation of the known flow velocity was an important part of this research effort. The post-processing routines were selected from within the Dantec FlowManager software program, and one goal of the project was to optimize the software settings for future work in the AFIT supersonic tunnels. This was accomplished concurrently throughout the image

acquisition process chronicled in the previous sections of this Chapter. There are general principles that can be applied to all types of images when using the Dantec FlowManager software for generating vector maps, however.

IV. Analysis and Results

Section 1 – Initial CO_2 Seeding Experiments and Vector Map Generation

Initial Experimental Seeding Runs

As mentioned in Chapter three, the first objective of this research was to demonstrate the ability to seed the Mach 2.9 flow with CO_2 particles after the wind tunnel system had been brought back online after an extended period of downtime. The image acquisition parameters entered into the Dantec FlowManager software are shown in Table 1. The initial experimental runs were conducted with the injection, camera, laser and software parameters shown in Table 2.

Table 2: Initial CO_2 seeding parameters

Parameter	Setting
Injector type	Multi-port
Injector placement	Converging-diverging nozzle sidewall
Injector orientation	Aligned with flow direction
Camera aperture setting	F-stop 8
Laser head position	Three inches from test section sidewall

In all images captured for this research, the flow travels from right to left through the illumination plane. Image pairs captured during these initial runs are shown in Figure 18 and Figure 19. It was initially unclear whether these images would be sufficient for successful vector map generation using the Dantec PIV system due to the non-uniformity of particle seeding and particle overexposure evident in the images. For the images shown in Figure 18 and Figure 19, the structure of the particle cloud is very clearly seen.

It is obvious that, for the illumination plane, the majority of the field of view of the camera did not contain visible particles. Additionally it is clear from these images, especially the first image in each image pair, that the light intensity from portions of the images is too great for the camera. This resulted in overexposure of the image, or washout. Regions of the image containing washout cannot provide any type of particle displacement data since image contrast is required to provide a clear correlation peak.

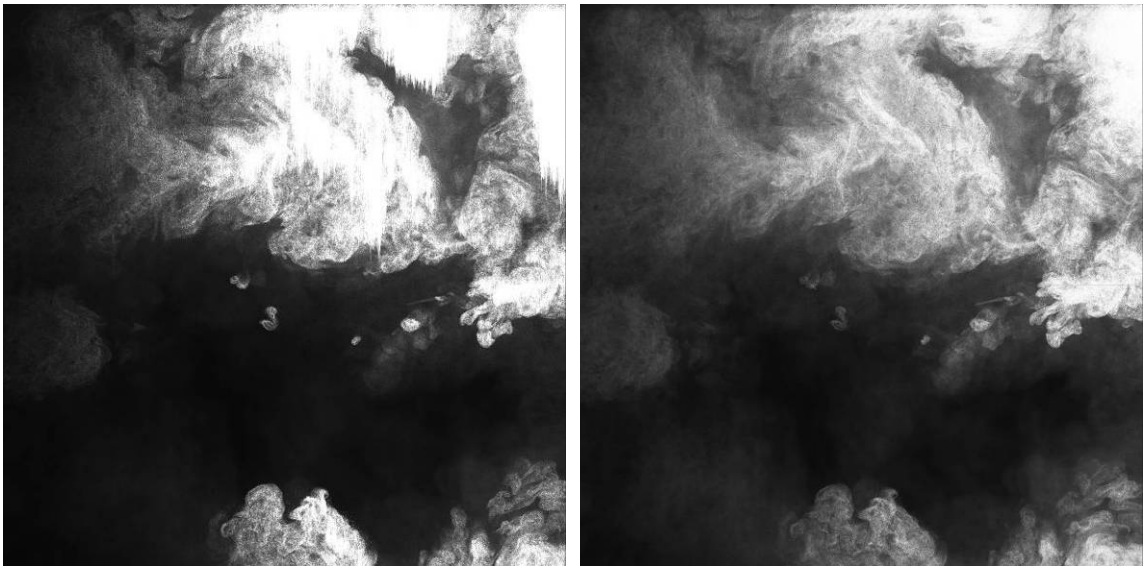

Figure 18: Image pair from initial CO2 seeding

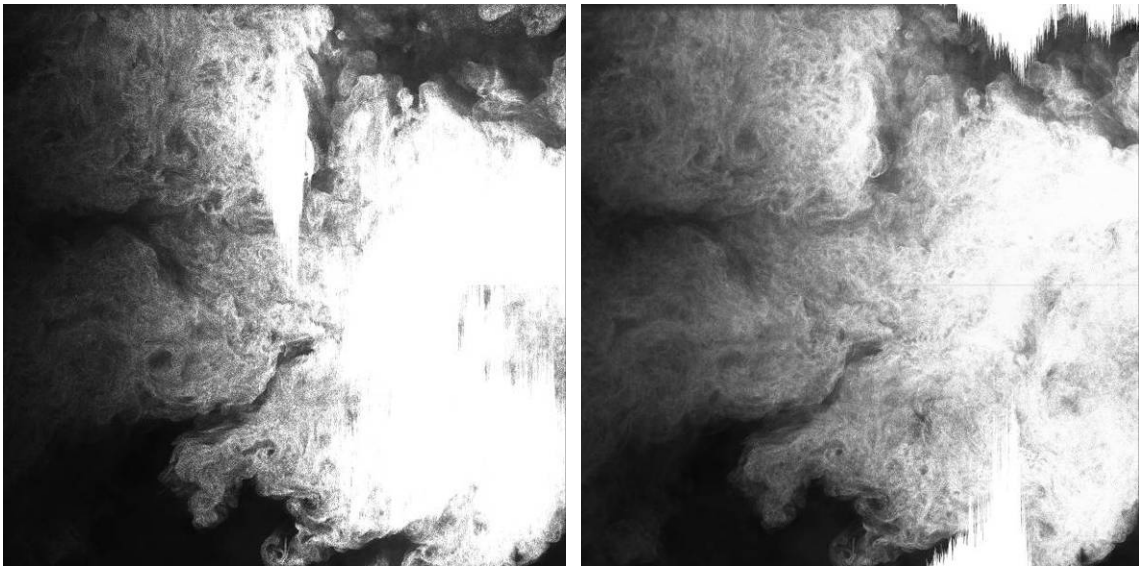

Figure 19: Image pair from initial CO2 seeding

It is also evident from these images that the first image in each image pair suffered greater washout than the second image. In addition, the second image in each image pair reveals more visible particles than the first image and a lower overall light intensity across the entire illumination plane. At this initial stage, it was unclear whether this reduction in light intensity from the first image to the second image would negatively impact the ability of the FlowManager system to generate accurate vector maps. It was clear, however, that the washout seen in these image pairs was unacceptable for PIV processing and had to be reduced or eliminated to enable successful vector map generation.

The four images shown in Figure 18 and Figure 19 are only a representative sample of the images generated during the initial experimental runs. The other images are quite similar to these four, with varying degrees of washout and particle density and uniformity within the illumination plane.

Initial Vector Map Generation

Inspection of Figure 18 reveals that this image pair is less than ideal for PIV processing due to uneven particle distribution and laser light intensity, however these initial images were processed using the Dantec FlowManager software to generate vector maps. The vector map shown in Figure 20 was generated using the single image pair from the initial seeding run shown in Figure 18. The program TecPlot 360 was used to process the FlowManager data file to create the image shown in Figure 20.

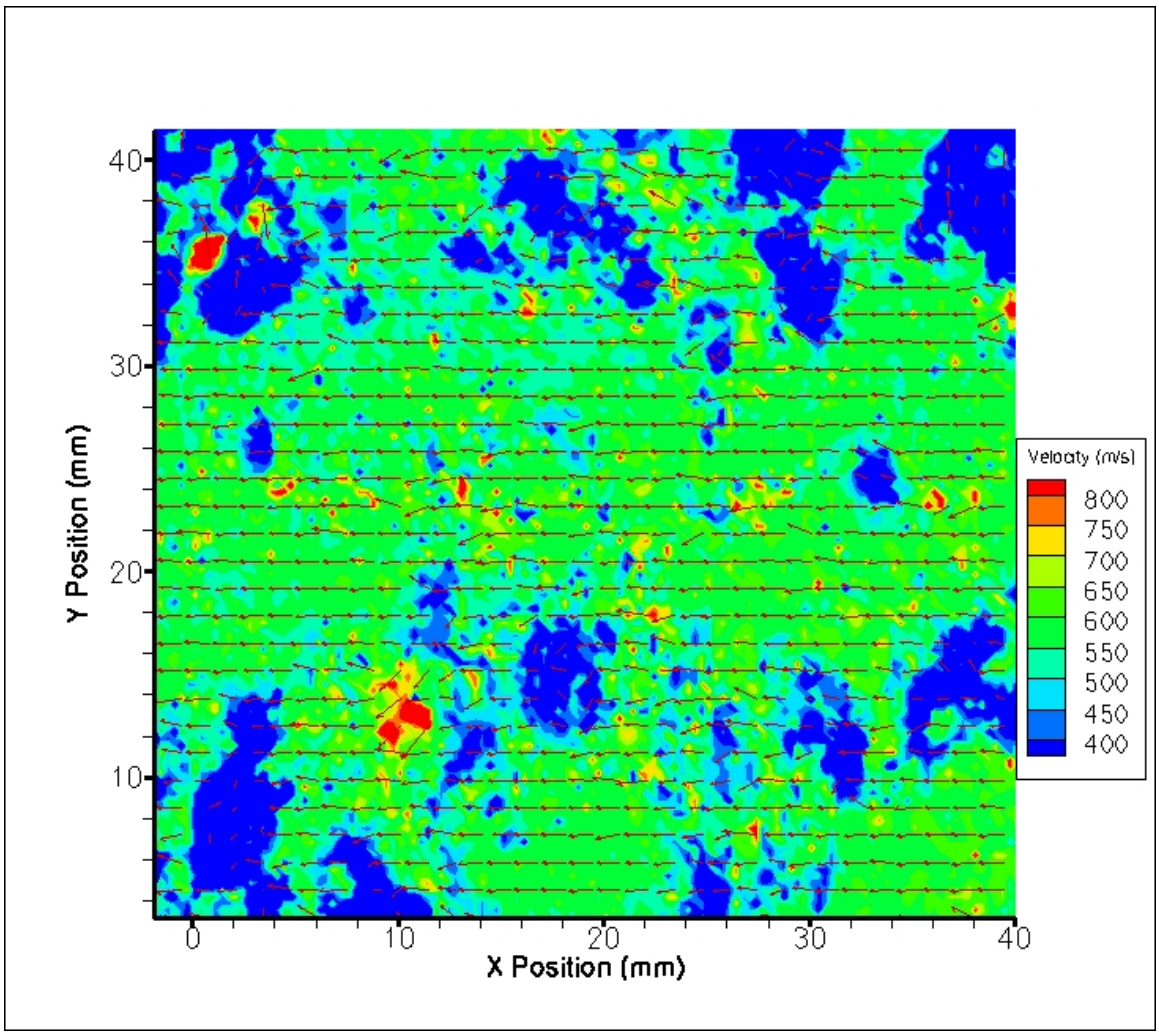

Figure 20: Vector Map generated from initial run

In Figure 20, the vectors are shown in black. The algorithm for generating the vector map shown in Figure 20 is given in Table 3. This algorithm was chosen after reading the FlowManager manual and speaking with a Dantec Dynamics representative.

Table 3: Initial FlowManager vector map generation algorithm

Parameter	Setting
Cross correlation method	Adaptive Correlation
Interrogation area size	Initial: 256x256 pixels Final: 32x32 pixels
Number of refinement steps	3
Number of calculation passes per step	2
Validation method	Moving Average validation

The adaptive correlation method involves the scaling of interrogation area sizes from larger to smaller, implementing FFTs for each size step, to refine vector generation for each interrogation area. In this case, three size steps were used, and two FFT calculation passes were made for each refinement step. Therefore, a total of six FFTs were completed for each interrogation area, and the final interrogation area of 64x64 pixels contained the vector generated by this adaptive correlation. It is important to note that only one in four vectors is shown in Figure 20 due to the high density of vectors in the original vector map.

After the adaptive correlation was completed and a vector was generated for each interrogation area, a vector validation was accomplished. The moving average validation method was chosen upon the recommendation of Dantec Dynamics. This method compares each vector with its nearest neighboring vectors, and if it is not sufficiently

similar to them it is then rejected. This level of similarity can be set within the FlowManager software. The comparison of vectors involves matching the FFT signal peaks for each vector, if the signal peak strength for a certain vector does not fall within a certain proximity range of its neighboring vector peaks, that vector is rejected. The software allows for rejected vectors to be substituted with value-averaged replacement vectors, and any further calculations can either include or ignore the substituted vector values.

The vector map shown in Figure 20 reveals a primarily right-to-left moving flow field, which is consistent with the flow direction in the test section. There are numerous spurious vectors in the vector map, many of which point in very different directions and with very different magnitudes. Again, the flow is traveling nominally at Mach 2.9, which translates to approximately 606 m/s for the test conditions based on isentropic flow assumptions (3). The majority of the vectors in the map are within the 550 m/s to 650 m/s range as illustrated by the color coding in the legend. There are, however, many pockets of higher and lower magnitude vectors with seemingly random orientations. This is caused by non-uniform particle seeding as there were large empty areas within the image pairs as well as regions which were effectively overexposed. Another concern was that the size of individual particles was at the sub-pixel level. As a result, the calculated velocities were likely based on the translation of large groups of particles. This is sufficient for uniform flow, but it is undesirable for general wind tunnel testing.

These low particle densities within the area of investigation lead to low signal to noise ratios. Therefore, the software may calculate a vector in an interrogation area quite erroneously based on the presence of very few particles, particles that move into or out of

the interrogation area or simply noise. In addition, the washout seen in the sample images was present in nearly all initial image pairs, and can greatly reduce the ability of the software to generate accurate vectors within interrogation areas that suffer from washout in one or both images of the image pair. These spurious vectors were to be encountered in large and small quantities throughout the duration of the experiments and calculations run in this research.

An encouraging result of this initial experiment was that the functionality of the PIV system was confirmed for a Mach 2.9 flow using a one microsecond delay time between pulses. However, it was clear that improved particle distribution would be required to fully exploit the PIV technique.

Section 2 – Refining Injection Technique, System Setup and Processing Method

Multi-port Injector in Nozzle Sidewall

The first change made to the experimental setup after the initial data was collected was changing the injection orientation of the multi-port nozzle. As shown in Figure 15, the injector was oriented with the direction of the flow, transverse 90˚ to the flow direction and directly opposed to the flow direction. The results of these runs are shown with the sample images in Figure 21 through Figure 24. It is important to note that each of the images in Figure 21 through Figure 24 is a sample image from a single image pair recorded during the experimental run. These images were selected for inclusion in this thesis because they are representative of the qualitative features of all the images in the data set for that particular run. The key features to note are the lighting exposure

throughout the image, the particle density within the illumination plane, the particle uniformity within the illumination plane and the individual particle sizes.

For the experimental run represented by the image in Figure 21, it is evident that there is still washout occurring in much of the image. This was a problem with nearly all of the images in that data set. Additionally, the particles are not uniformly filling the illumination plane, but are instead collected in clusters leaving large empty areas in the illumination plane. Finally, in areas that do not suffer from washout, it is evident that the particles are very small and very closely packed. All three of these issues make this set of images less than ideal for PIV processing. For this run, the experimental parameters were set according to Table 4.

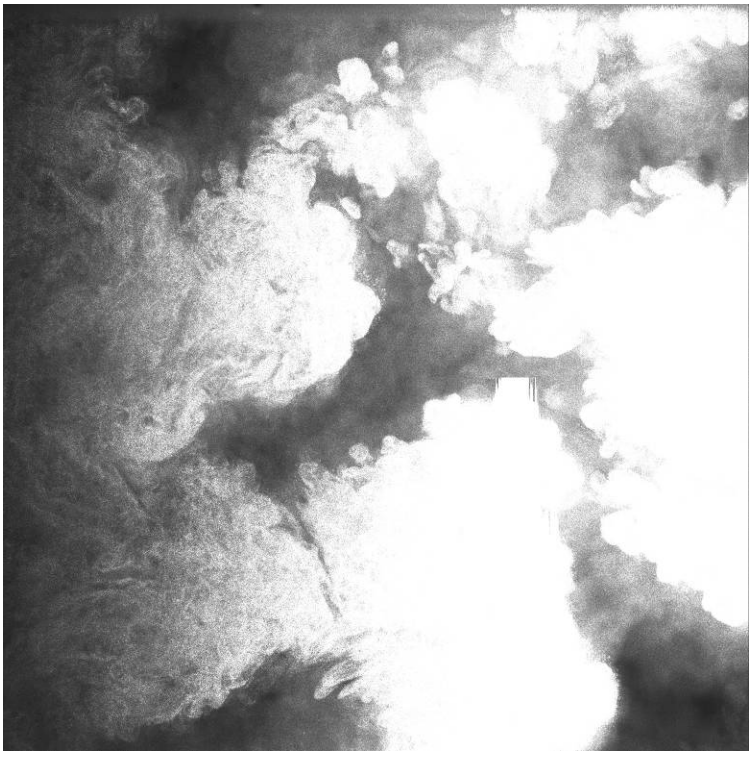

Figure 21: Multi-port injection in flow direction

Table 4: Experimental parameters for multi-port injection in flow direction

Parameter	Setting
Injector type	Multi-port
Injector placement	Converging-diverging nozzle sidewall
Injector orientation	Aligned with flow direction
Camera aperture setting	F-stop 8
Laser head position	Three inches from test section sidewall

The images collected from this experimental run were analyzed using the FlowManager software with the same procedural steps used in the initial CO_2 seeding run described earlier in this Chapter. The resulting vector maps were similar to those generated for the initial seeding run shown in Figure 20. For those image pairs with severe washout, no amount of altering the FlowManager algorithm enabled the generation of useful vector maps. It is evident that washout is the most problematic issue encountered throughout these experiments; particle density, uniformity and size can affect the generation of useful vector maps, but these problems can be solved to a great extent with by changing the FlowManager algorithm. Washout, however, is a problem that the software cannot handle, even with the variation of processing parameters.

For the next run, the injector was rotated in its mount so that CO_2 was injected in a direction opposing the flow, as illustrated in Figure 15. The set of images collected in this run is represented by the image shown in Figure 22. The experimental parameters for this run are shown in Table 5.

Figure 22: Multi-port injection reverse to flow direction

Table 5: Experimental parameters for multi-port injection reverse to flow direction

Parameter	Setting
Injector type	Multi-port
Injector placement	Converging-diverging nozzle sidewall
Injector orientation	Aligned reverse to flow direction
Camera aperture setting	F-stop 8
Laser head position	Three inches from test section sidewall

Changing the injector orientation did not improve the images much for the purposes of PIV processing. As shown in Figure 22, when compared to Figure 21, there seems to be even more washout. It appears that the particles are more uniformly

distributed throughout the illumination plane, but there are still significant areas in which there are few particles present, if any at all. There are still particle structures present, in which particles are clustered together. The image pairs from this experimental run were not suitable for the generation of useful vector maps. Multiple FlowManager algorithms were used in an attempt to process these image pairs, but the generated vectors were quite random in both orientations and magnitudes. The vector map generated from the image pair containing the image in Figure 22 is shown in Figure 23. This vector map was generated with the FlowManager algorithm described in Table 6.

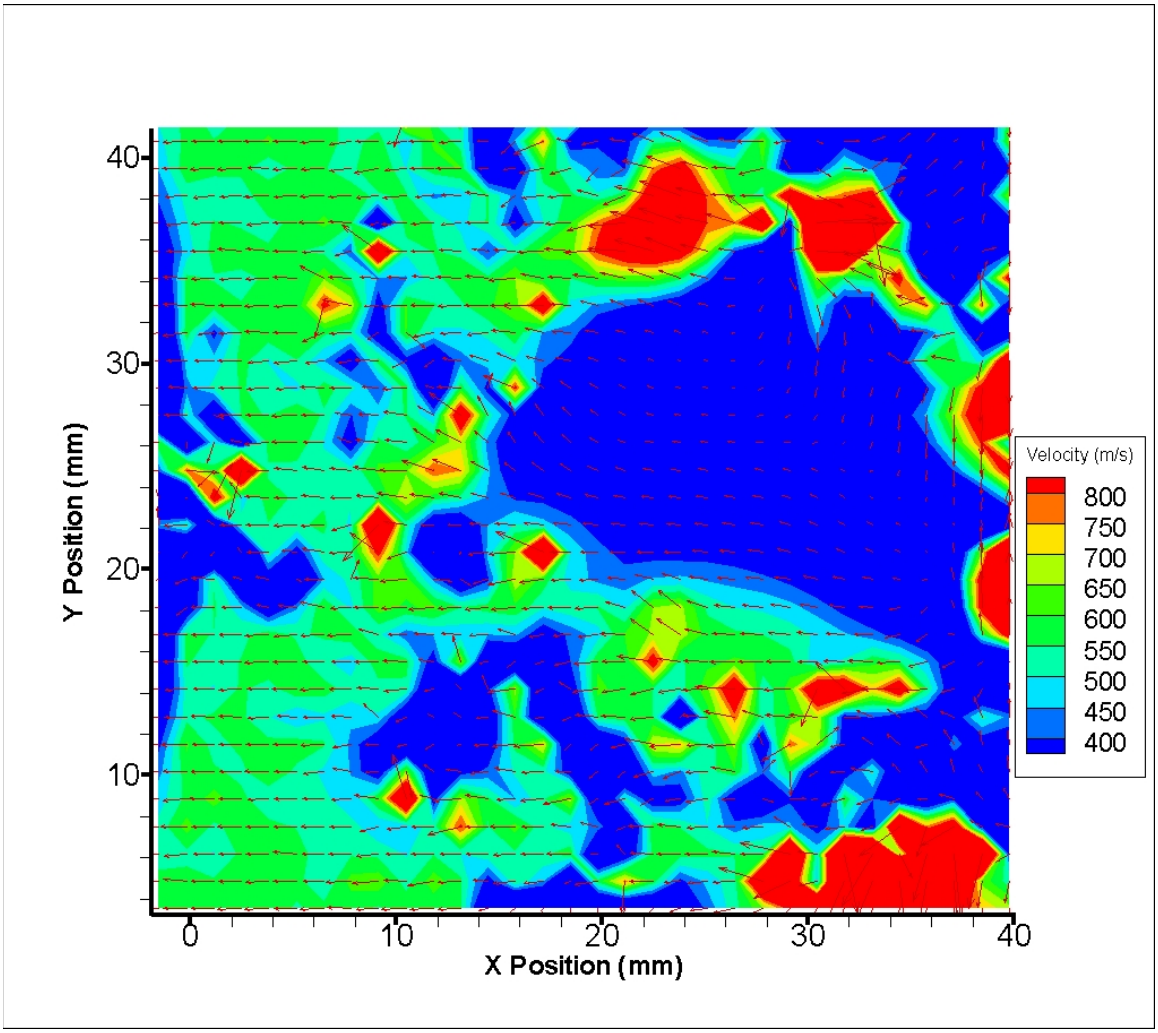

Figure 23: Vector map generated from injecting reverse to flow direction

Table 6: FlowManager algorithm used for multi-port injection reverse to flow direction

Parameter	Setting
Cross correlation method	Adaptive Correlation
Interrogation area size	Initial: 256x256 pixels Final: 32x32 pixels
Number of refinement steps	3
Number of calculation passes per step	2
Validation method	Moving Average validation

The vector map shown in Figure 23 does contain many vectors that are shown in the proper right-to-left orientation and in a realistic velocity range near 600 m/s. There are, however, many other vectors which are neither oriented in the expected direction nor of the proper magnitude. In some areas, the vectors are of far greater magnitudes than the expected value and oriented in nearly the opposite direction from the expected direction. The algorithm used to generate this vector map, described in Table 6, is the product of an optimization process in which the different algorithm parameters were varied to achieve the most realistic vector map generation possible. Many prior combinations of algorithm parameters were attempted that yielded vector maps that were exceedingly random.

Once again, the washout present in the images collected from injecting reverse to the flow direction in the nozzle sidewall location no doubt contributed heavily to the unsuitability of these images for PIV processing. For nearly all image pairs, excessive washout and densely packed particles were likely the main factors in the inability of any FlowManager algorithm to generate realistic, useful vector maps.

For the final experimental run with the multi-port injector located in the nozzle sidewall, the injection orifices were turned so that the CO_2 was injected transversely up 90˚ from the direction of the flow. This injector orientation is illustrated in Figure 15. A representative image from the resulting set is provided in Figure 24, and the experimental parameters for this run are given in Table 7.

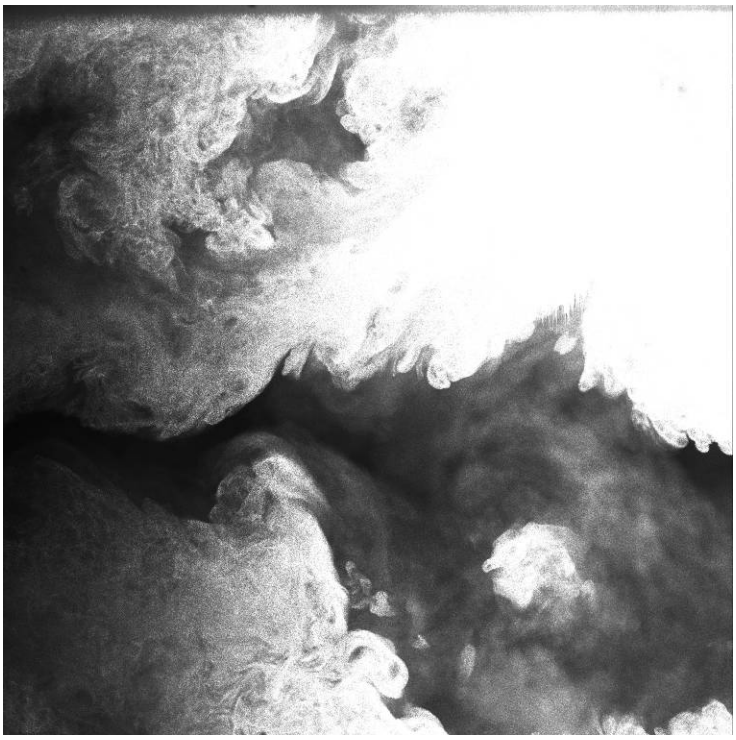

Figure 24: Multi-port injection transverse to flow direction

Table 7: Experimental parameters for multi-port injection transverse to flow direction

Parameter	Setting
Injector type	Multi-port
Injector placement	Converging-diverging nozzle sidewall
Injector orientation	Aligned transverse up to flow direction
Camera aperture setting	F-stop 8
Laser head position	Three inches from test section sidewall

It is once again evident that many of the particles illuminated by the laser are overexposed. There are many particle structures that are clearly visible in Figure 24, which lead to clusters of particles as well as many areas with little to no particle presence. These factors once again made realistic vector map generation extremely difficult.

An important factor in maintaining the aperture setting at F-stop 8 was the desire to avoid speckle, a phenomenon described in Chapter three. The aperture was kept as open as practical for each experiment, with an F-stop value of 8 considered the most closed setting suitable for this research. Aperture settings any more closed than F-stop 8, without using a light filter, produced images that were overexposed due to excessive particle density. Ideally, the aperture would be kept completely open, which for the camera lens used here would be an F-stop value of 2.8. Since overexposure occurs when the aperture is left too open, a fully open setting is not always possible. In later experiments using the shroud injector, a Melles Griot model 03-FV-038 filter with 18% light transmission at the 532 nm wavelength was used to enable the aperture to be set

wide open without overexposing the images. The results of using the filter are presented in a following section.

After reviewing each of the three multi-port injector orientations described in this section, it was evident that larger individual particle sizes would be beneficial to meaningful vector map generation. In addition, increased particle uniformity throughout the illumination plane would improve the quality of the vector maps by providing information throughout the entire area of investigation. And, obviously, reducing the amount of washout was a critical improvement to be achieved so that robust measurements could be performed.

Multi-port injector in Stagnation Chamber

After the preceding orientations were explored using the multi-port injector in the nozzle sidewall injection location, the injector was moved to the stagnation chamber injection location. The purpose in moving the injector to this location was to attempt to improve particle dispersal throughout the illumination plane and acquire greater particle uniformity by allowing the particles a longer time and distance to fill the entirety of the test section. Since the free stream flow velocity is very low in the stagnation chamber, it was expected that the CO_2 particles would more fully disperse throughout the flow.

Multiple experimental runs were accomplished using the multi-port injector in the stagnation chamber injection location. Two different injector orientations were investigated. In addition, camera aperture settings and laser head positions were varied in an attempt to generate the best possible vector maps.

The first two experiments were conducted with the injector oriented to inject CO_2 in the same direction as the flow. The experimental parameters for these two runs are shown in Table 8 and Table 9.

Table 8: Experimental parameters for multi-port stagnation chamber injection, run 1

Parameter	Setting
Injector type	Multi-port
Injector placement	Top of stagnation chamber
Injector orientation	Aligned with flow direction
Camera aperture setting	F-stop 4
Laser head position	Three inches from test section sidewall

Table 9: Experimental parameters for multi-port stagnation chamber injection, run 2

Parameter	Setting
Injector type	Multi-port
Injector placement	Top of stagnation chamber
Injector orientation	Aligned with flow
Camera aperture setting	F-stop 8
Laser head position	Three inches from test section sidewall

For the first experiment in the stagnation chamber injection site, the aperture was opened to an F-stop value of 4 to let in more light than an F-stop value of 8. A

representative image from the set of image pairs collected during this run is given in Figure 25.

Figure 25: Multi-port injection in stagnation chamber with flow, run 1

It is apparent from this representative image that the flow field has a much more uniform dispersal of particles than when the multi-port injector was placed in the nozzle sidewall. However, the particle size seems to be smaller than when using the prior injection site. Also, the problem of overexposure is still present in this set of image pairs.

An additional problem surfaced during this experimental run. As illustrated in Figure 26, the laser sheet did not illuminate the particles consistently from the first image to the second image in the image pair. The illumination of particles from image 1 to image 2 causes the particles to appear to be moving from left to right. In fact, the

particles are moving from right to left, but the illusion is created by the brightest portion of the laser sheet for image 1 hitting the particles to the left of where the laser sheet hits for image 2. The movement of light in the illumination plane tricks both the eye of the observer and the FlowManager software into believing that it is in fact particles that are moving left to right, when this is actually not the case. This is a problem that will be addressed later in this section.

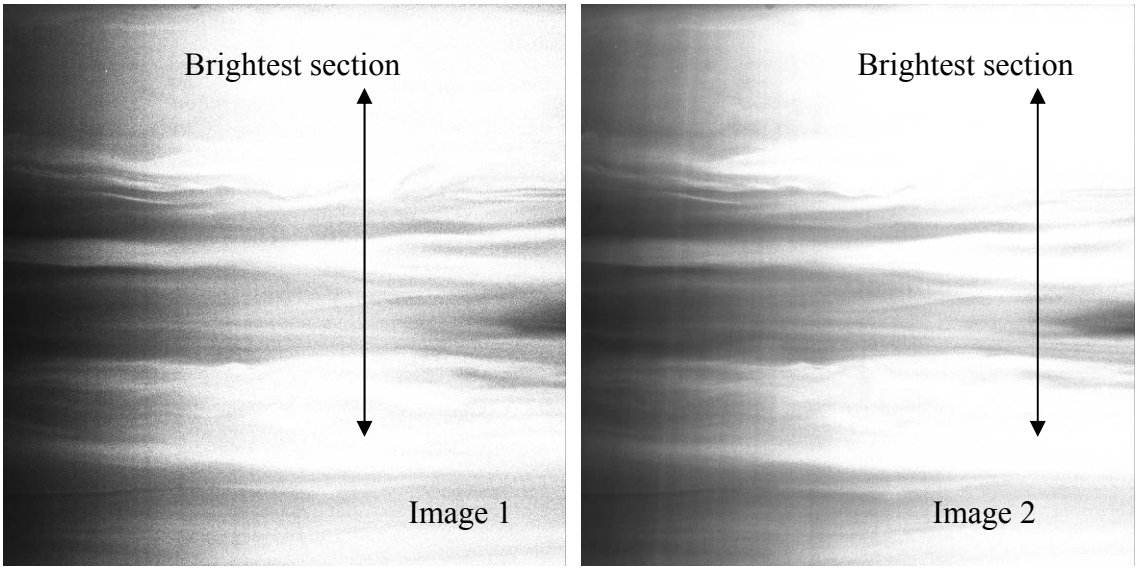

Figure 26: Image pair from multi-port injection in stagnation chamber, run 1

As a result of the misleading lighting condition from image 1 to image 2 in each image pair, as well as the overexposure and small particle sizes present in the images it was not possible to generate meaningful vector maps for any of the images in this experimental run. To attempt to remedy the lighting problems from run 1 with the injector in the stagnation chamber, the aperture was set from F-stop 4 to F-stop 8 for run 2 in accordance with Table 9. As shown in the representative image pair in Figure 27, this did reduce the amount of overexposure in the images for run 2 tremendously. The

particles are still quite small, but they are not overexposed. However, it is evident that the same problem of false left-to-right particle motion is encountered with these images.

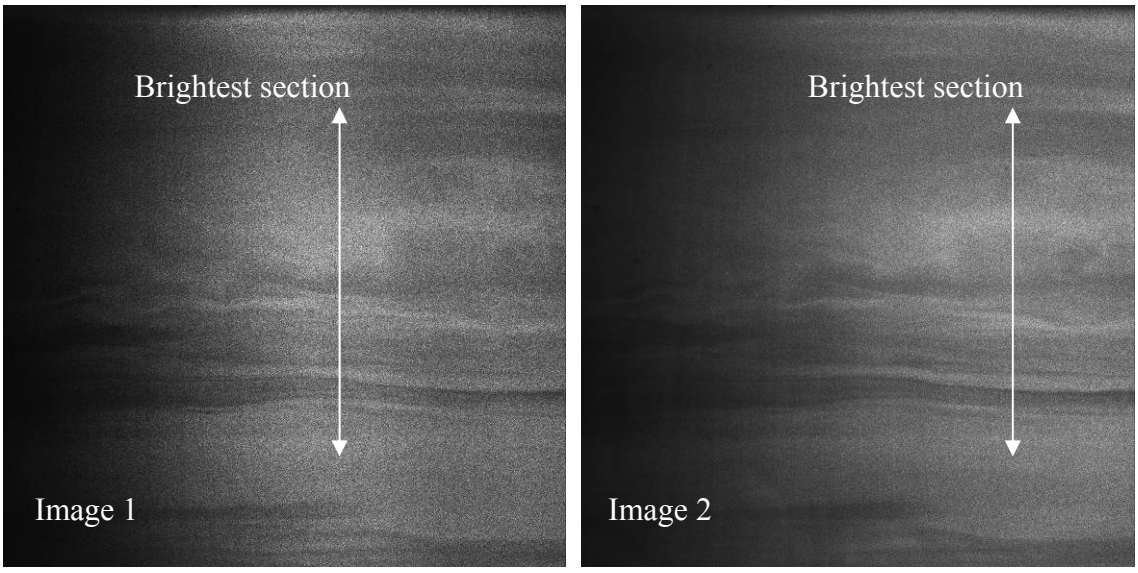

Figure 27: Image pair from multi-port injection in stagnation chamber, run 2

As a result of the increased visibility of particles due to increased particle contrast, the FlowManager software was able to generate vectors that were more smooth and consistent than the completely random vectors generated from the image pairs of run 1. This only compounded the problem posed by the false left-to-right particle motion, however, and the vectors generated from the image pairs of run 2 were in near total opposition to the known direction of the flow. There were areas in the vector map, as with previous runs, where the vectors were oriented in more realistic directions and magnitudes. The vast majority, though, were obviously spurious and not meaningful in any way.

To attempt to resolve the issue of laser sheet misalignment, for run 3 the laser head was moved one inch farther away from the test section wall to reduce the light intensity in the illumination plane. In addition to this change, the aperture was opened

back up to the same setting as run 1. The injector was also oriented to inject CO_2 reverse to the direction of the flow. The experimental parameters for run 3 are listed in Table 10.

Table 10: Experimental parameters for multi-port stagnation chamber injection, run 3

Parameter	Setting
Injector type	Multi-port
Injector placement	Top of stagnation chamber
Injector orientation	Reverse to the direction of flow
Camera aperture setting	F-stop 4
Laser head position	Four inches from test section sidewall

A representative image pair from run 3 is given in Figure 28. It is obvious that these images are useless for PIV processing due to the excessive washout of the particles in the illumination plane.

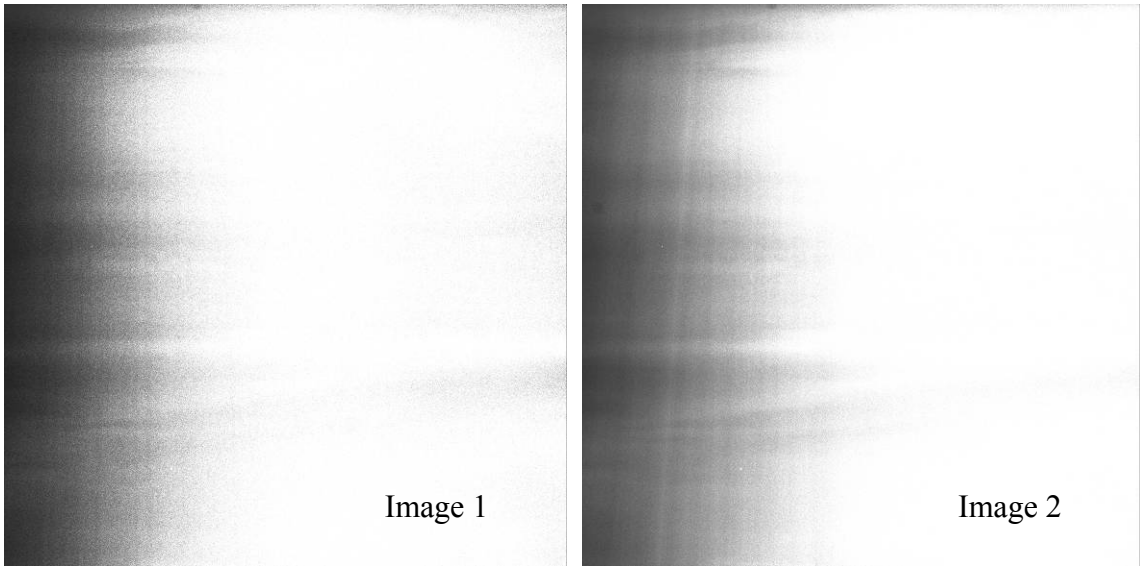

Figure 28: Image pair from multi-port injection in stagnation chamber, run 3

Though it is difficult to distinguish individual particles from the image pair in Figure 28, it appears that reversing the injection orientation to oppose the direction of the flow caused the particle size in the test section to decrease. This is expected, since the particles would have a longer residence time in the flow prior to reaching the illumination plane and, thus, more time to sublimate from the solid state into the gaseous state. It is notable in Figure 28 that the laser sheet's left-to-right shift is still present.

For the next run with the multi-port injector in the stagnation chamber, run 4, the aperture was closed slightly. The experimental parameters are shown in Table 11. A representative image pair from this run is shown in Figure 29. The image pairs collected in this experimental run generated results very similar to run 2, with the apparent left-to-right particle motion causing the generation of incorrect vector maps.

Table 11: Experimental parameters for multi-port stagnation chamber injection, run 4

Parameter	Setting
Injector type	Multi-port
Injector placement	Top of stagnation chamber
Injector orientation	Reverse to the direction of flow
Camera aperture setting	F-stop 5.6
Laser head position	Four inches from test section sidewall

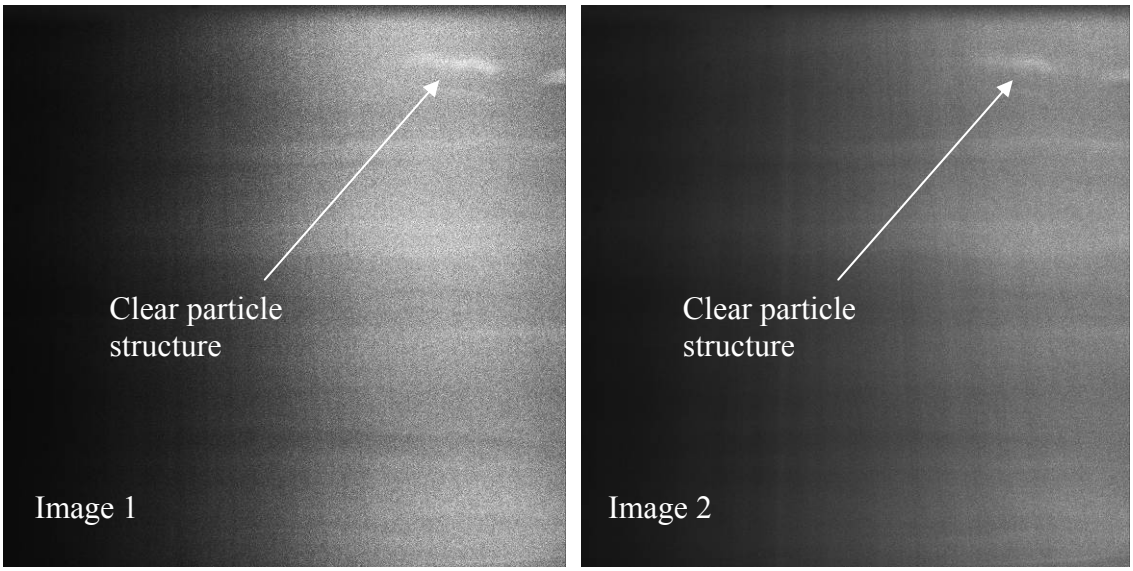

Figure 29: Image pair from multi-port injection in stagnation chamber, run 4

From Figure 29 it is apparent that closing the aperture from run 3 to 4 greatly reduced the washout seen in Figure 28. The upper right regions of these images contain a clear particle structure which can be observed to translate in the appropriate right-to-left direction. Unfortunately, the remainder of the measurement plane did not lead to correct

velocity measurements using the FlowManager software. Additionally, moving the laser head farther from the test section caused the laser sheet misalignment from laser pulse 1 to pulse 2 to be increased. This misalignment was due to imperfect orientation of mirrors within the laser. Properly aligning the two individual laser beams inside the New Wave Research Solo 120 laser is possible, but was postponed until other forms of troubleshooting were attempted. Since placing the laser head closer to the tunnel test section reduces the amount of relative misalignment between pulse 1 and 2, the corrective action chosen was to move the laser head even closer than its original location.

In addition to the inconsistent lighting problem, the particle sizes resulting from injecting with the multi-port injector in the stagnation chamber injection location are undesirable. The small size of these particles makes it very difficult to analyze the images for the generation of realistic and meaningful vector maps. Upon the recommendation of Dantec Dynamics, it was determined that larger particles would be much more useful for successful PIV processing.

Shroud Injector in Stagnation Chamber

To increase the particle size in the test section, it was decided to use the shroud injector shown in Figure 7. According to a collaborative effort between AFIT and Innovative Scientific Solutions Incorporated, allowing the solid particles to agglomerate before entry into the flow field has been a successful method of increasing CO_2 particle size for PIV injection. To that end, the shroud injector was designed to allow the CO_2 particles to reside in the shrouded portion of the injector after exiting the 0.030 inch inside diameter feed tube at the entrance of the shroud tube. The stagnation chamber

injection site was used first to enable comparison to the results of injection with the multi-port injector in that same location. A similar method of growing CO_2 particles for cleaning is marketed by Vatran (6).

The experimental parameters for runs 1 and 2 with the shroud injector at the stagnation chamber injection site are given in Table 12 and Table 13, respectively. The Melles Griot model 03-FV-038 filter was used during these runs to allow the camera aperture to be set at its most open setting, for an F-stop value of 2.8.

Table 12: Experimental parameters for shroud injection into stagnation chamber, run 1

Parameter	Setting
Injector type	Shroud
Injector placement	Top of stagnation chamber
Injector orientation	Tube exit approximately two inches deep in stagnation chamber
Camera aperture setting	F-stop 2.8
Laser head position	Four inches from test section sidewall
Filter	Melles Griot, 18% transmission at 532 nm

Table 13: Experimental parameters for shroud injection into stagnation chamber, run 2

Parameter	Setting
Injector type	Shroud
Injector placement	Top of stagnation chamber
Injector orientation	Tube exit approximately two inches deep in stagnation chamber
Camera aperture setting	F-stop 2.8
Laser head position	Two inches from test section sidewall
Filter	Melles Griot, 18% transmission at 532 nm

The images captured from runs 1 and 2 using the shroud injector in the stagnation chamber injection site were extremely dark. Having moved the laser head two inches closer to the tunnel test section between runs 1 and 2, it was expected that the light intensity for run 2 would be greater than that of run 1. This was the case, but the light intensity was not increased sufficiently to successfully illuminate the CO_2 particles for PIV processing. The images collected from run 2 were still far superior to the nearly completely dark images from run 1. One of the best image pairs from run 2 is shown in Figure 30.

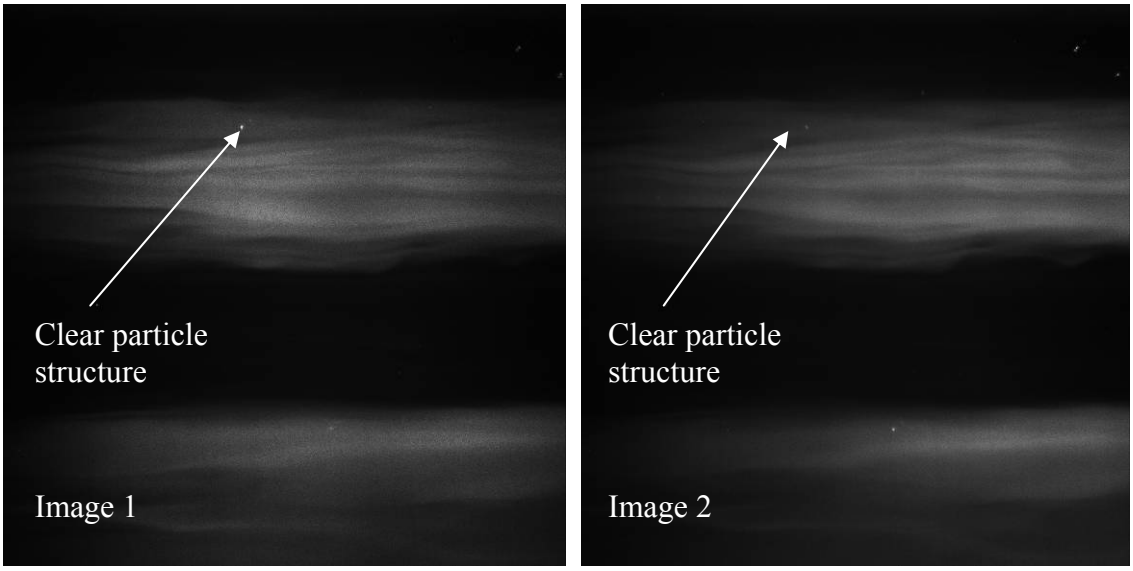

Figure 30: Image pair from shroud injection in stagnation chamber, run 2

It is clear from the images in Figure 30 that the quality of the image pairs captured using the shroud injector at the stagnation chamber injection site were not suitable for PIV processing. The overwhelming majority of particles appear to be dispersed in a fog-like pattern, with large empty spaces throughout most of the image. A clearly visible particle structure is visible in the upper left portion of each image, as shown in Figure 30, which appears to follow the proper right-to-left flow direction despite the apparent left-to-right motion due to laser sheet misalignment. The majority of the image pairs collected from runs 1 and 2 contained far fewer visible particles than the images in Figure 30, making these experimental runs unsuitable for processing into vector maps. It was determined that to increase the particle sizes in the test section, the shroud injector should subsequently be placed at the nozzle sidewall injection site. The particles would then have a shorter residence time in the flow, with the desire being that they would not sublimate to the extent that they did when injected in the stagnation chamber.

Shroud Injector in Nozzle Sidewall

For the remainder of the experiments conducted for this research, the shroud injector was utilized at the nozzle sidewall injection site. The initial placement of the shroud injector into the nozzle sidewall and the subsequent first experimental run were conducted according to the parameters in Table 14.

Table 14: Experimental parameters for shroud injection into nozzle sidewall, run 1

Parameter	Setting
Injector type	Shroud
Injector placement	Converging-diverging nozzle sidewall
Injector orientation	Tube exit approximately two inches beyond mounting sidewall inner face
Camera aperture setting	F-stop 2.8
Laser head position	Two inches from test section sidewall
Filter	Melles Griot, 18% transmission at 532 nm

The resultant image pairs from the setup described in Table 14 were of far greater usefulness for PIV processing than those captured while using the shroud injector at the stagnation chamber injection site. A sample image pair from experimental run 1 is shown in Figure 31.

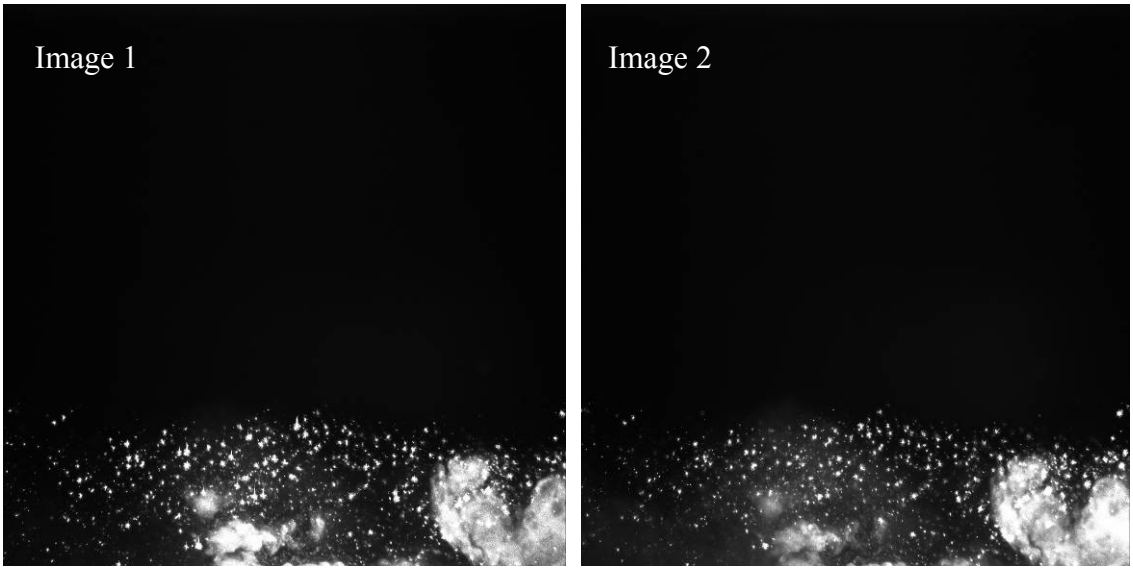

Figure 31: Image pair from shroud injection in nozzle sidewall, run 1

It can be clearly seen in Figure 31 that there are two distinct modes of visible particles, those in a fog-like pattern and those in large, discrete particles. Without question, the more desirable of these two modes is the discrete particle. The image pair shown in Figure 31 is representative of the image pairs collected during run 1, with some of the image pairs displaying more fog-like areas and some displaying mostly discrete particles. Regardless of the particle mode, the CO_2 present in the images from run 1 was located near the lower boundary of the image, which corresponds to the inner face of the test section sidewall opposite the sidewall in which the injector was mounted. This indicates that the CO_2 particles remained near the far sidewall after exiting the shroud injector, and did not disperse uniformly throughout the test section after entering the flow in the nozzle.

It was decided to adjust the mounting assembly for the shroud injector to place the exit of the injector more near the inner face of the nozzle sidewall in which it was mounted. The exit of the shroud injector was moved to approximately ¾ inch from the

inner face of the mounting sidewall with the desire that the momentum of the CO_2 particles as they exited the injector would cause them to disperse uniformly throughout the width of the test section. Additionally, the laser head was moved one inch farther from the test section. The following experimental run, run 2, was conducted according to the parameters in Table 15.

Table 15: Experimental parameters for shroud injection in nozzle sidewall, run 2

Parameter	Setting
Injector type	Shroud
Injector placement	Converging-diverging nozzle sidewall
Injector orientation	Tube exit approximately ¾ inch beyond mounting sidewall inner face
Camera aperture setting	F-stop 2.8
Laser head position	Three inches from test section sidewall
Filter	Melles Griot, 18% transmission at 532 nm

The following figures are sample image pairs from the set collected during experimental run 2 injecting with the shroud injector in the nozzle sidewall.

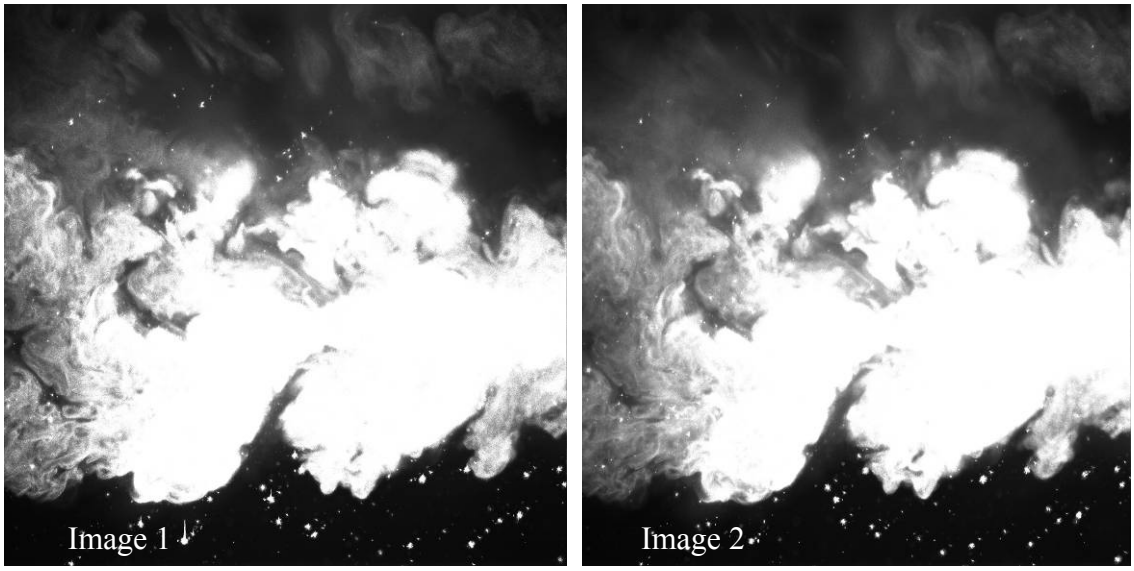

Figure 32: Image pair from shroud injection in nozzle sidewall, run 2

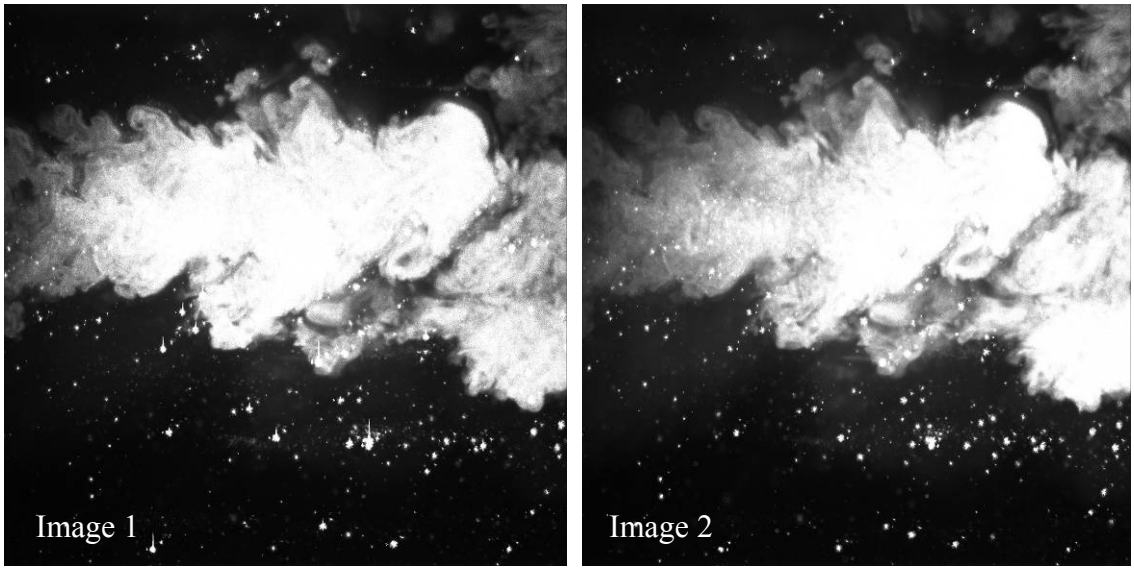

Figure 33: Image pair from shroud injection in nozzle sidewall, run 2

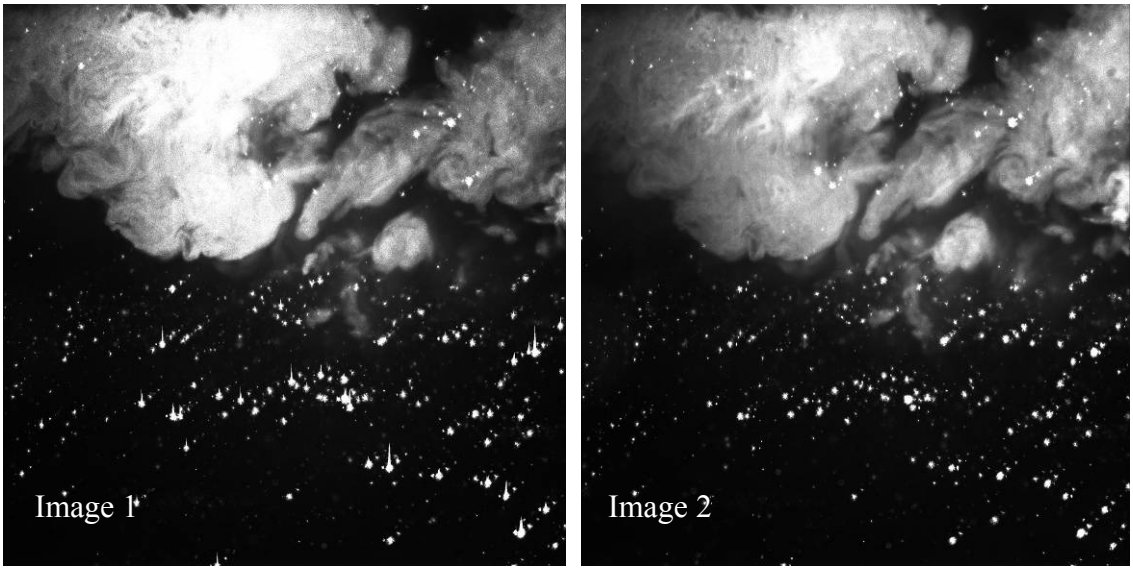

Figure 34: Image pair from shroud injection in nozzle sidewall, run 2

The particle uniformity across the width of the test section was greatly improved from run 1 to run 2, as shown in Figure 32, Figure 33 and Figure 34. The two modes of particle consistency are still present in the images from run 2. With the abundance of discrete particles present in these images, processing them with the FlowManager software to generate vector maps was accomplished successfully, especially in the lower half of the illumination plane. The following figures are the resultant vector maps generated from each of the image pairs shown in Figure 32, Figure 33 and Figure 34. Table 16 shows the FlowManager algorithm used to generate these vector maps.

Table 16: FlowManager algorithm used to generate vector maps from Figure 32, Figure 33 and Figure 34

Parameter	Setting
Cross correlation method	Adaptive Correlation
Interrogation area size	Initial: 512x512 pixels Final: 64x64 pixels
Number of refinement steps	3
Number of calculation passes per step	2
Validation method	Moving Average validation

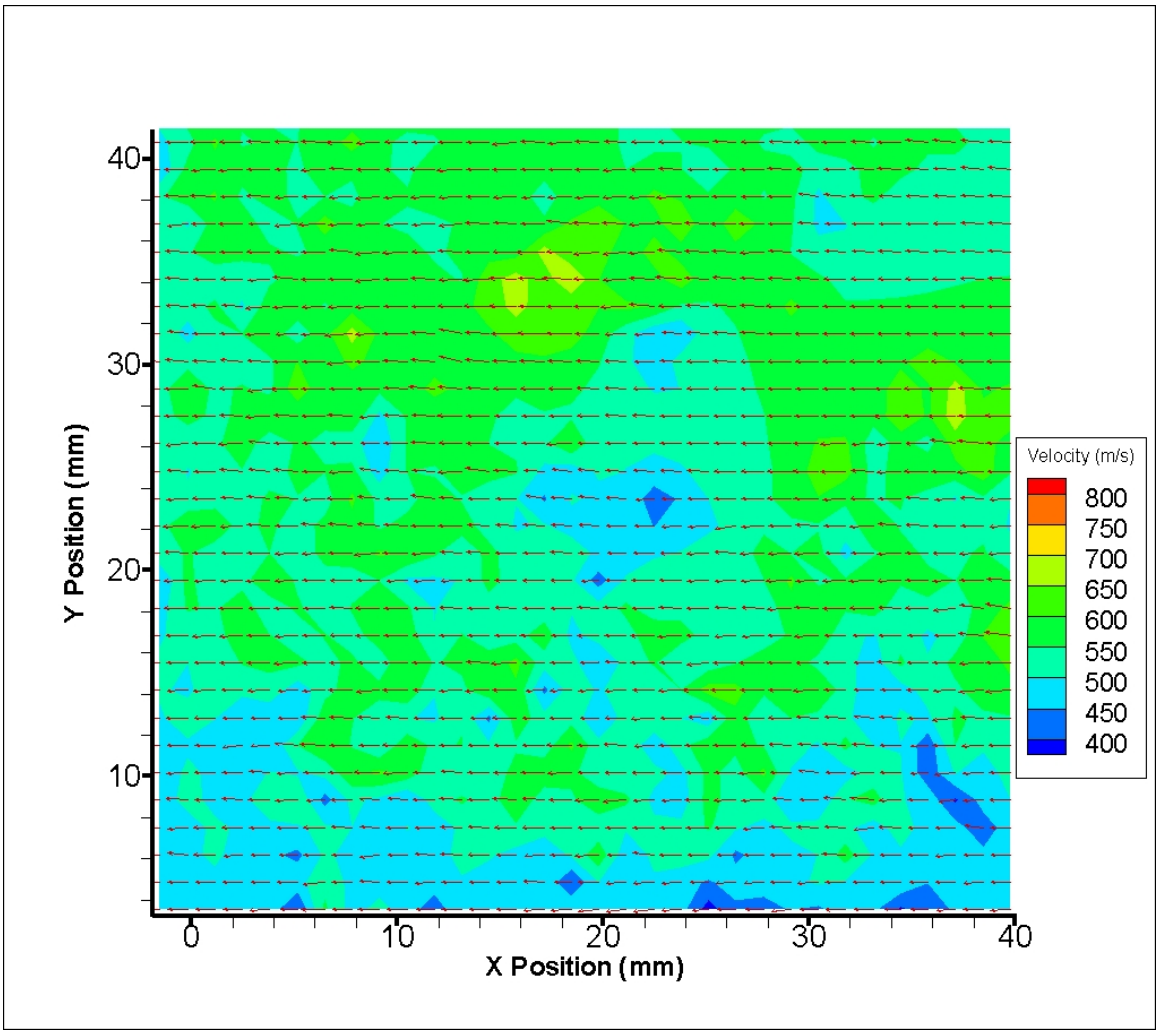

Figure 35: Vector map generated from image pair shown in Figure 32

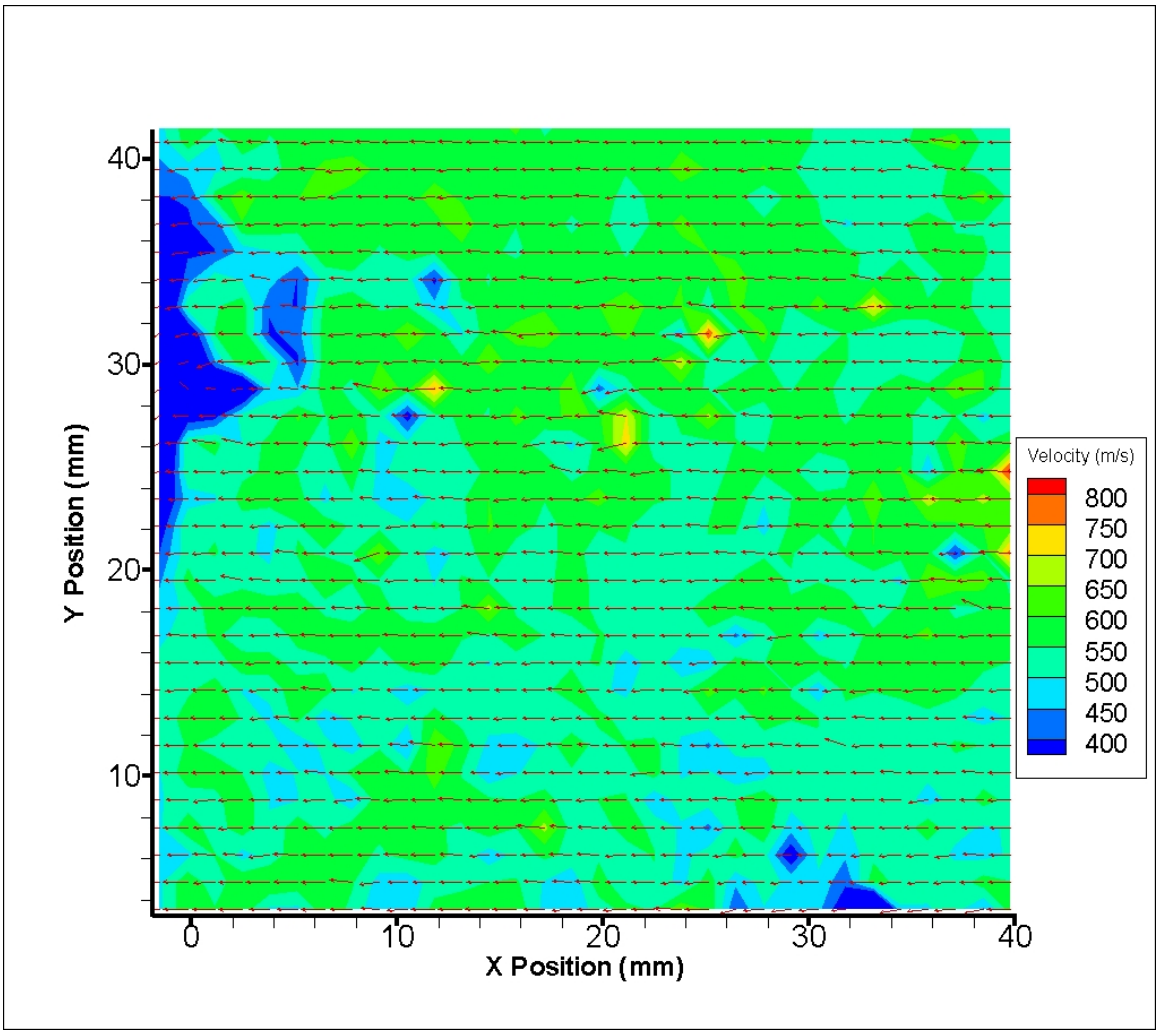

Figure 36: Vector map generated from image pair shown in Figure 33

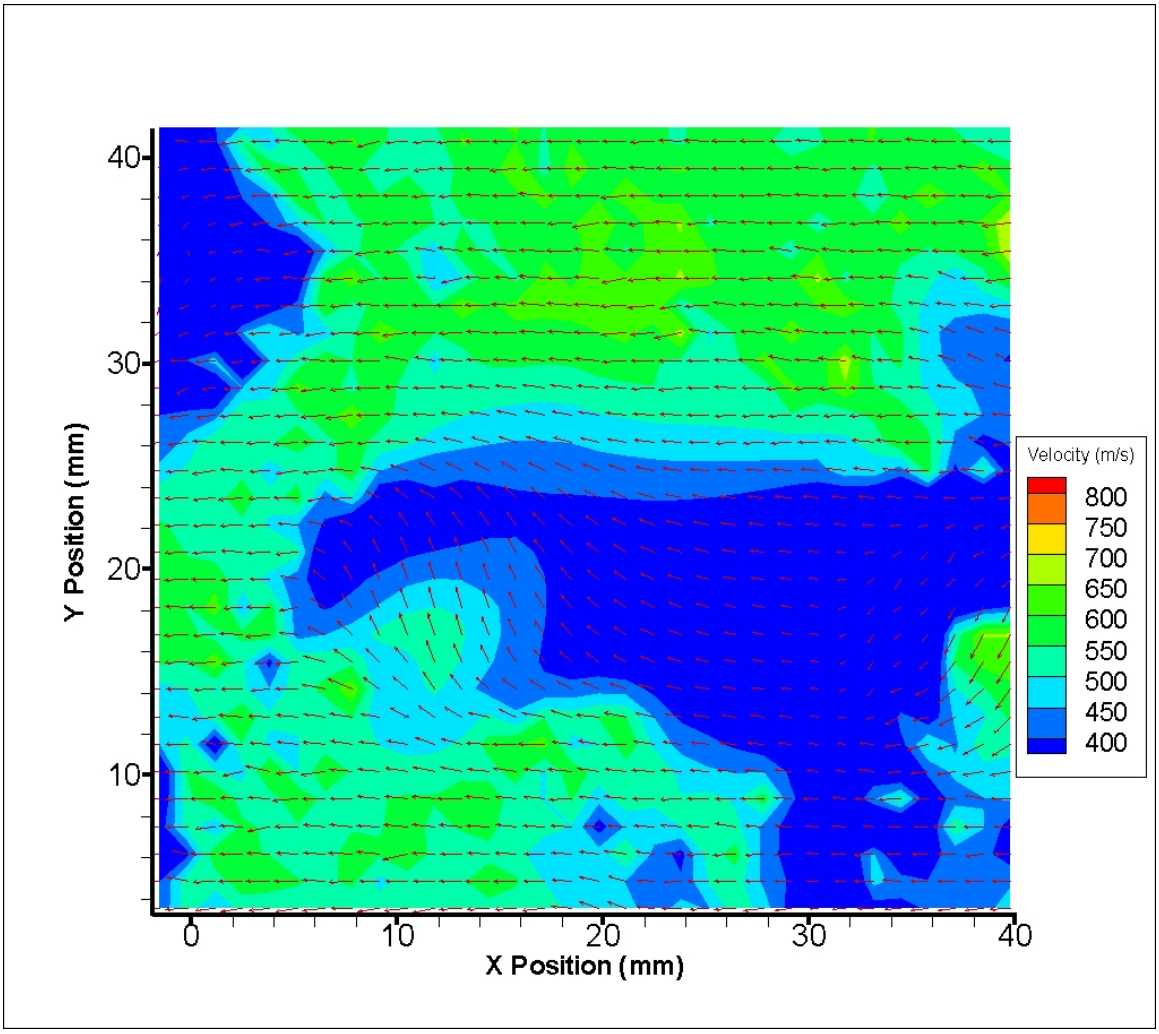

Figure 37: Vector map generated from image pair shown in Figure 34

The discrete particles visible in the image pair samples shown in Figure 32, Figure 33 and Figure 34 were overexposed to varying degrees. In addition, the fog-like particle clouds led to washout. The laser head was moved back an inch between runs 1 and 2 to alleviate this problem, but this solution was not completely effective. One observation was that the imprecise alignment of the laser sheet was a higher order effect, and therefore no alignment improvements were performed in the course of this research.

It was observed during experimental run 2 that the mounting hardware that attached the 0.030 inch inside diameter feed tube to the 0.19 inch inside diameter shroud tube and mounted the injector to the nozzle sidewall was loose. Subsequently, CO_2 was ejected through the coupling assembly into the atmosphere during the experiment. Upon attempting to tighten the coupler and mount, it was determined that the 0.030 inch inside diameter feed tube needed to be replaced. A 0.020 inch inside diameter feed tube was chosen to replace the 0.030 inch tube, and this smaller feed tube was used throughout the rest of the experiments run in this research.

From Figure 35, Figure 36 and Figure 37 it is evident that more accurate vector maps in regions where discrete particles were observed were generated from injecting with the shroud injector in the nozzle sidewall versus using the multi-port injector at either location. Figure 35 and Figure 36 in particular show very good uniformity of vector magnitudes and directions. The majority of the vectors shown in these figures are within close proximity to the isentropic prediction of 606 m/s velocity, and the vast majority of the vectors in these figures are aligned in the right-to-left orientation of the flow field in the wind tunnel test section. Figure 37, on the other hand, contains a large region in which the vector magnitudes are much lower than expected. What is surprising is that when the vector map in Figure 37 is compared with the image pair in Figure 34, the region of the vector map that contains the lower than expected velocities corresponds to the region of the image pair that contains predominantly discrete particles. This is counter to expectations, in which discrete particles are believed to be more suitable for accurate vector map generation. It is possible that the particle overexposure in that area of the image pair is causing the generation of spurious vectors. In addition, upon careful

examination of the images collected in this run, it appears that the discrete particles may in fact be slightly out of focus, causing them to be distorted from their actual appearance. Camera focus was not altered until the test section was disassembled for the insertion of a model in the tunnel, which is discussed later in this section.

Even considering the regions of the vector maps from run 2 that contain vectors that do not match the expected velocity and direction of the flow, the vector maps produced from the image pairs collected in run 2 adhered more closely to expectations than all those generated previously.

For experimental run 3 with the shroud injector in the nozzle sidewall, the experimental parameters were set according to Table 17. It is important to reiterate that the feed tube for the shroud injector had been changed from the initial 0.030 inch inside diameter tube to the replacement 0.020 inch inside diameter tube for this and all subsequent experiments. A sample set of image pairs collected during run 3 follows Table 17.

Table 17: Experimental parameter for shroud injection in nozzle sidewall, run 3

Parameter	Setting
Injector type	Shroud
Injector placement	Converging-diverging nozzle sidewall
Injector orientation	Tube exit approximately ¾ inch beyond mounting sidewall inner face
Camera aperture setting	F-stop 2.8
Laser head position	Three inches from test section sidewall
Filter	Melles Griot, 18% transmission at 532 nm

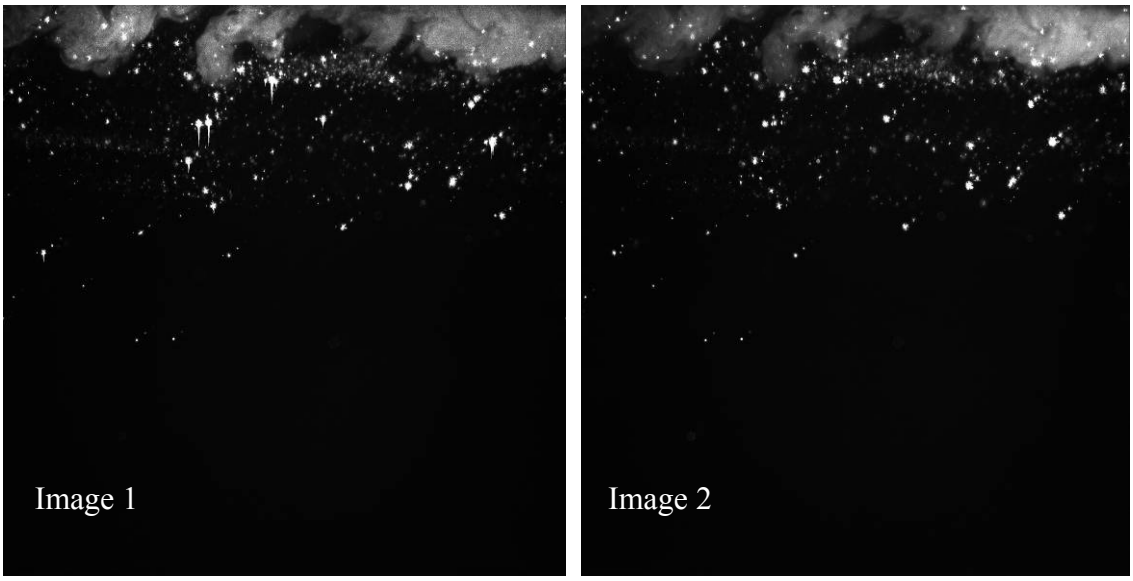

Figure 38: Image pair from shroud injection in nozzle sidewall, run 3

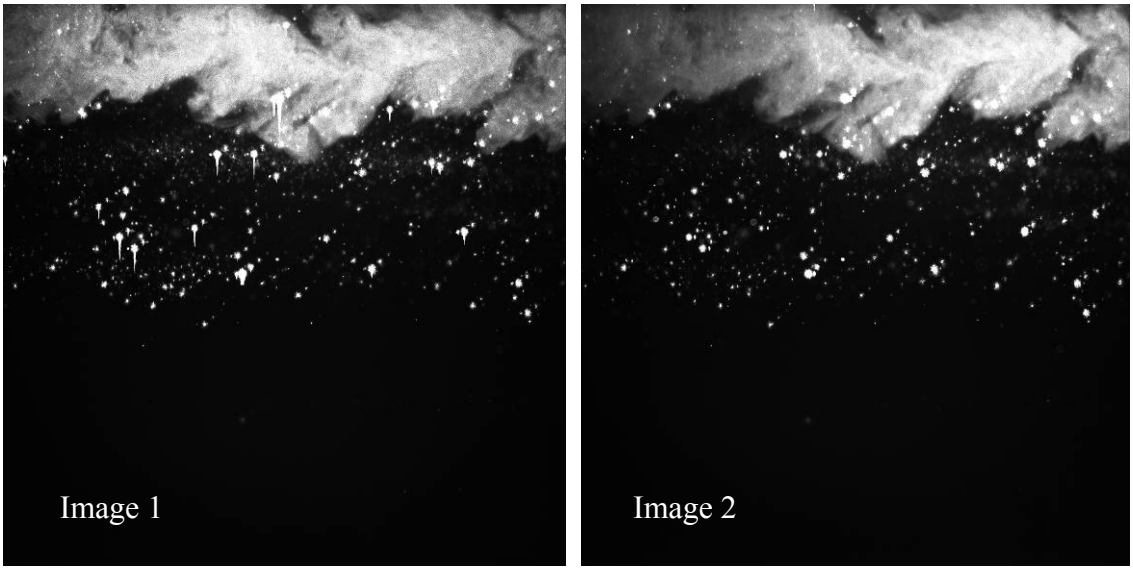

Figure 39: Image pair from shroud injection in nozzle sidewall, run 3

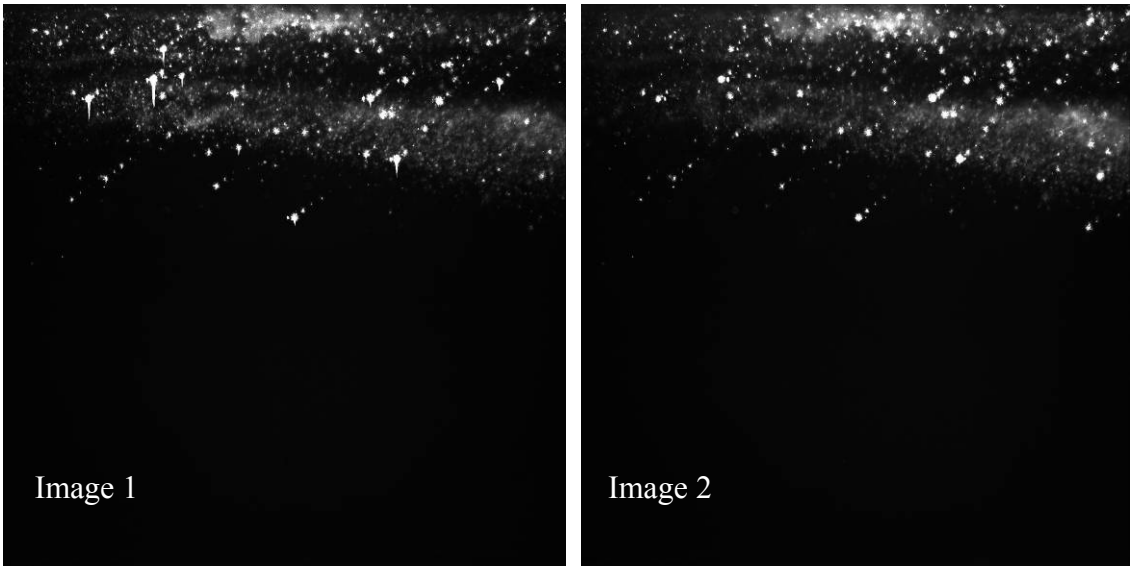

Figure 40: Image pair from shroud injection in nozzle sidewall, run 3

One clear difference between the images from run 3 and those from run 2 is that the particles did not disperse throughout the illumination plane as far in run 3 as they did in run 2. This is presumed to be due to the change in the inside diameter of the feed tube from 0.030 inch to 0.020 inch. The reduction in feed tube diameter most likely caused a reduction in the velocity of the CO_2 exiting the shroud injector into the flow, and thus the particles did not travel across the width of the tunnel test section as far as they had when injected using the larger feed tube.

There is still overexposure present for the discrete particles visible in Figure 38, Figure 39 and Figure 40. Additionally, the fog-like clouds are still present along with the discrete particles in these image pairs. Unfortunately, a CO_2 leak was still observed from the coupling hardware for the feed tube and the shroud tube at the nozzle sidewall injection site during this experimental run. This hardware was tightened again in preparation for the next run.

Vector maps were generated from the images in Figure 38, Figure 39 and Figure 40 and are shown in Figure 41, Figure 42 and Figure 43. The FlowManager algorithm used to generate these vector maps is the same as the algorithm provided in Table 16. This algorithm provided results most consistent with the expected velocity of 606 m/s for the flow field and right-to-left vector orientation. This algorithm would be used for all subsequent vector map generation.

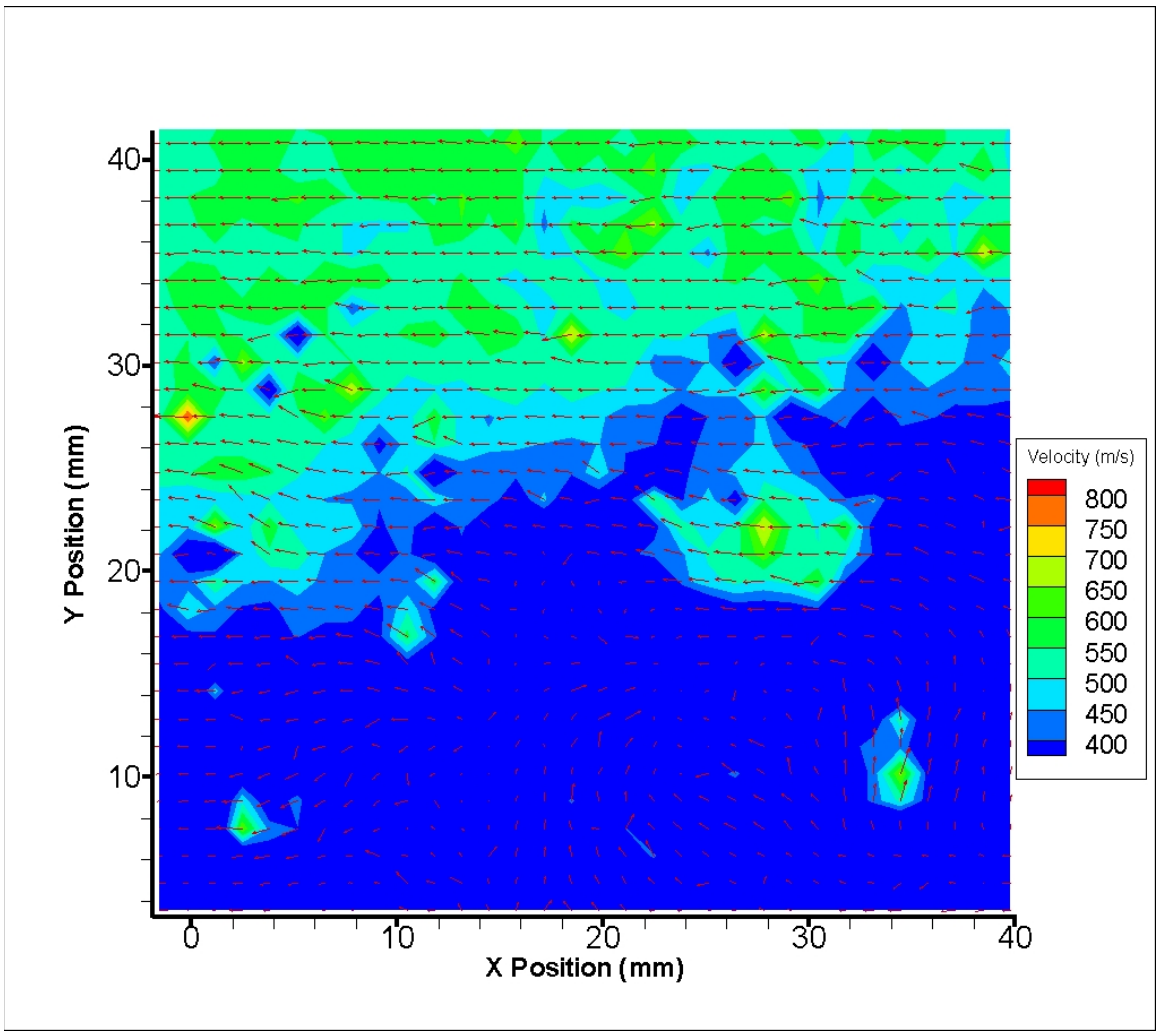

Figure 41: Vector map generated from image pair shown in Figure 38

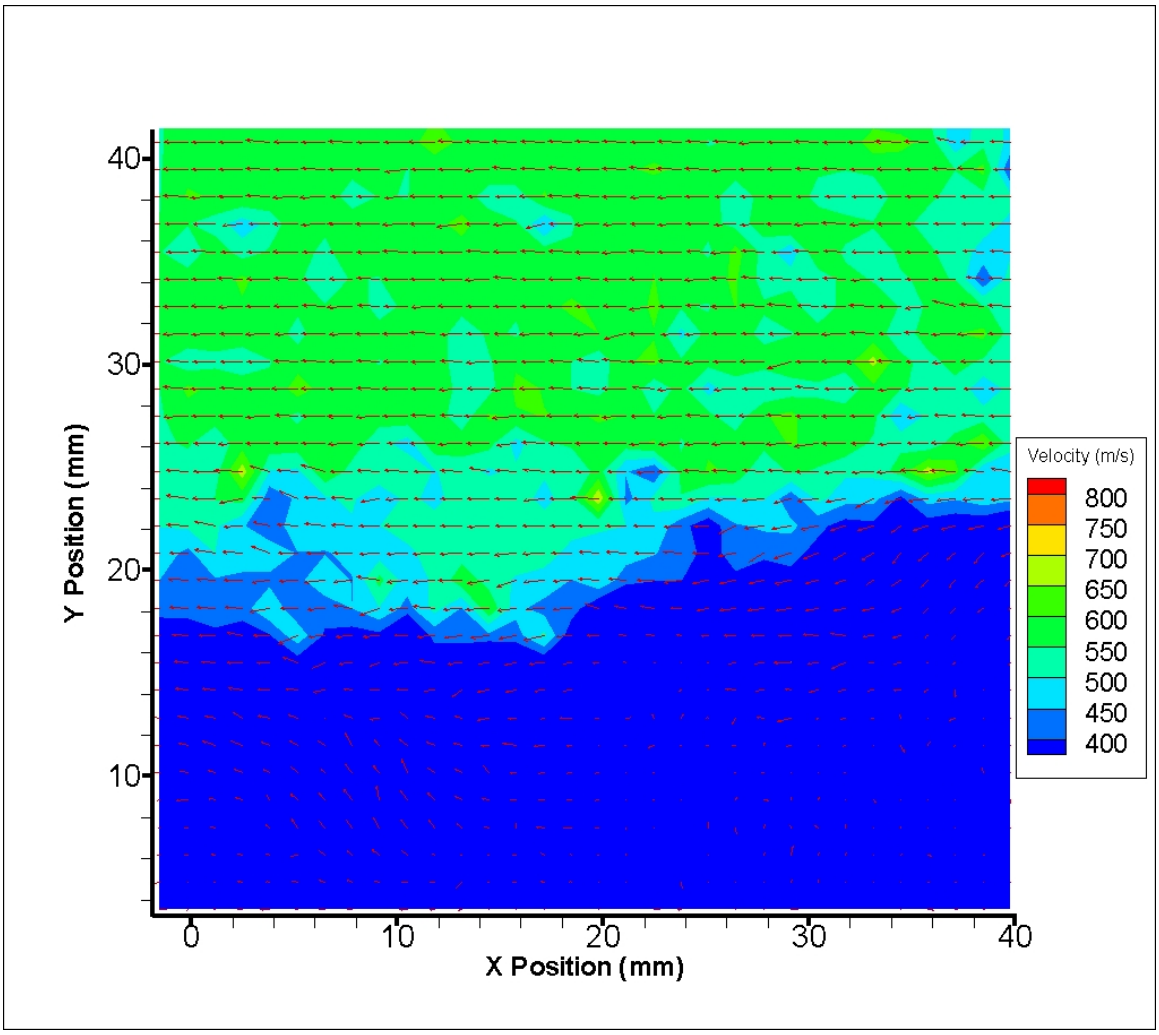

Figure 42: Vector map generated from image pair shown in Figure 39

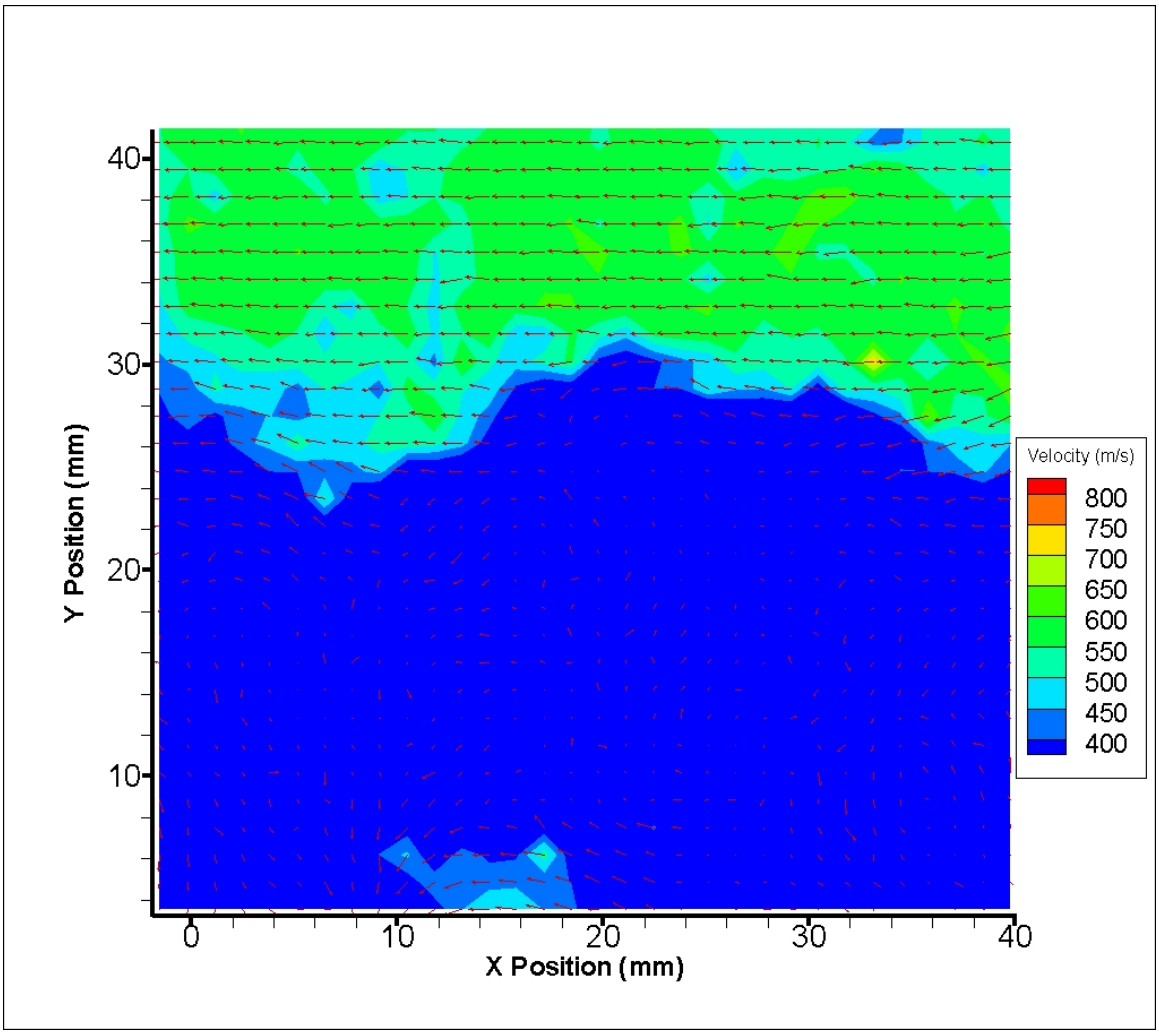

Figure 43: Vector map generated from image pair shown in Figure 40

It is quite clear from the vector maps provided in Figure 41, Figure 42 and Figure 43 that the areas of the image pairs that are devoid of particles are very apparent when viewing the corresponding vector map. Where the particles are present in the image pairs, however, the resultant vector maps in Figure 41, Figure 42 and Figure 43 are very close to the expected velocity and direction of the flow field. The slight reduction in particle seeding uniformity due to the change in feed tubes was undesirable, but it could be improved by moving the location of the shroud injector exit. For the purposes of this

research, the injector was left in the current configuration for the duration of the experiments to follow. Also, an illumination plane that only exhibits particle seeding in a certain portion of the flow field can be beneficial in future experiments if the area of investigation is the portion of the illumination plane that is seeded well.

From the three experiments conducted with the shroud injector in the nozzle sidewall injection site, the resulting vector maps represented the known flow field quite accurately wherever particles were present in the images collected. Having demonstrated the ability of the Dantec FlowManager software to successfully process realistic vector maps from images collected with CO_2 particle seeding, it was decided to insert a model of a 10˚ half-angle cone into the tunnel test section, as shown in Figure 8. Also, the camera was refocused more precisely to optimize the imaging process.

After the camera was refocused to the plane of laser sheet illumination, an experiment was conducted with the cone model in the wind tunnel test section. The experimental parameters for this run are provided in Table 18. This experimental run was actually conducted after a metal block was placed between the light arm and the test section window to prevent background scattering off the model. In addition to this precaution, the camera lens aperture setting was changed from F-stop 2.8 to F-stop 4 to further reduce the potential for light reflected from the cone model to interfere with the images collected and to improve the focus.

Table 18: Experimental parameters for shroud injection in nozzle sidewall, with model

Parameter	Setting
Injector type	Shroud
Injector placement	Converging-diverging nozzle sidewall
Injector orientation	Tube exit approximately ¾ inch beyond mounting sidewall inner face
Camera aperture setting	F-stop 4
Laser head position	Three inches from test section sidewall
Filter	Melles Griot, 18% transmission at 532 nm
Model in wind tunnel	10˚ half-angle cone model

A representative image pair from the set of images collected during this experiment is shown in Figure 44. An expanded, more detailed view of the second image in this image pair is shown in Figure 45.

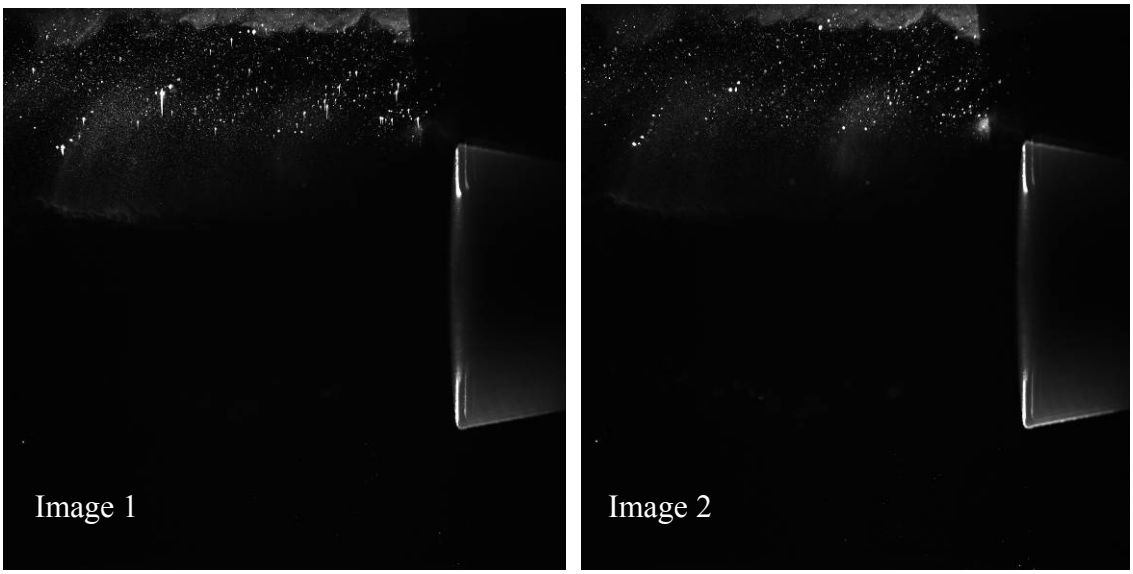

Figure 44: Image pair from shroud injection in nozzle sidewall, with model

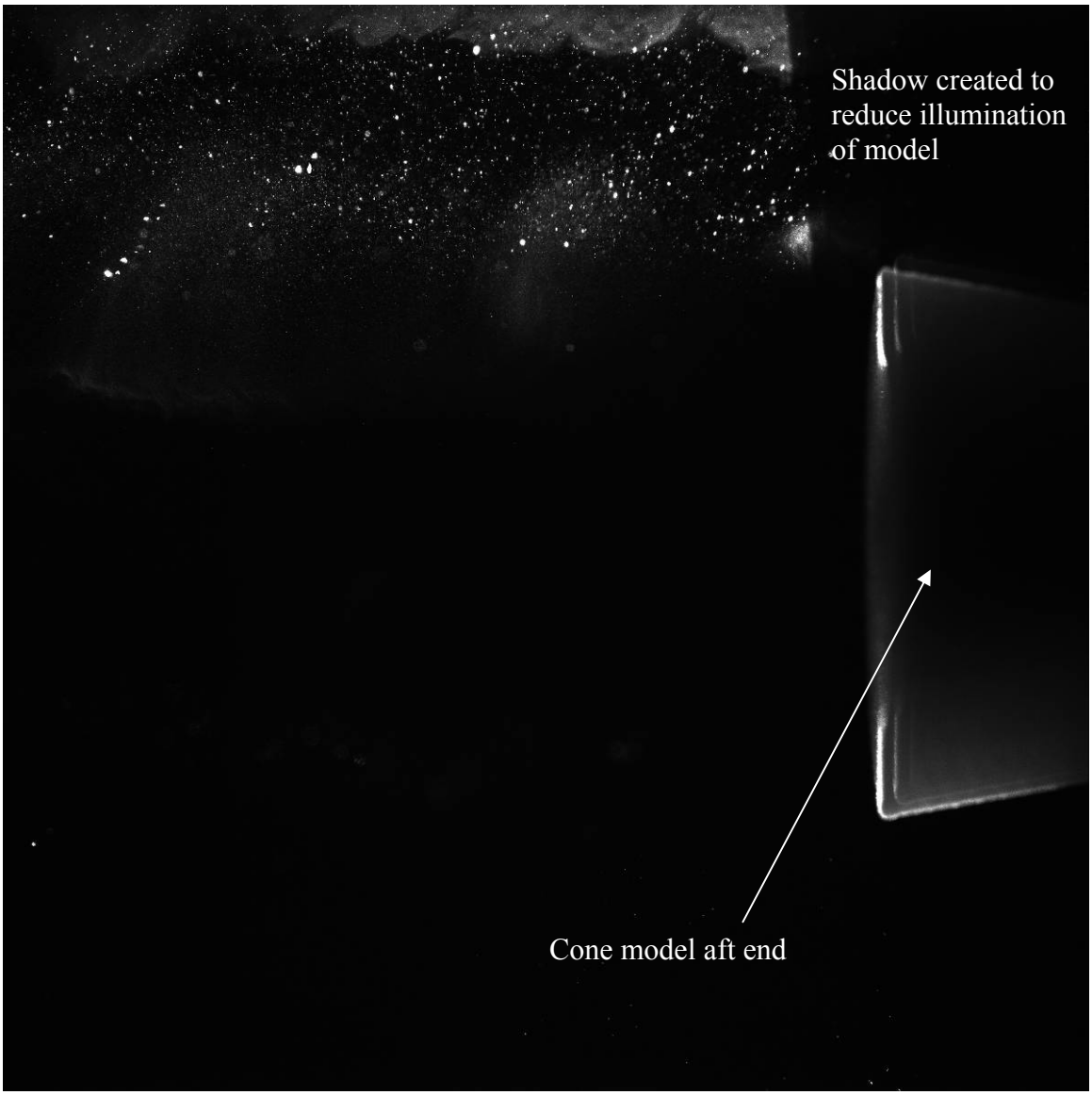

Figure 45: Expanded view of second image from Figure 44

The discrete particles visible in the images shown in Figure 44 and Figure 45 are sharper and clearer than the particles that are visible in any of the images collected from previous experiments using the shroud injector. The fine density of the discrete particles combined with their sharpness and detail in the images make these images very suitable for PIV processing. The image pair shown in Figure 44 was processed using the same algorithm described in Table 16

Table 16, and the resulting vector map is provided in Figure 46.

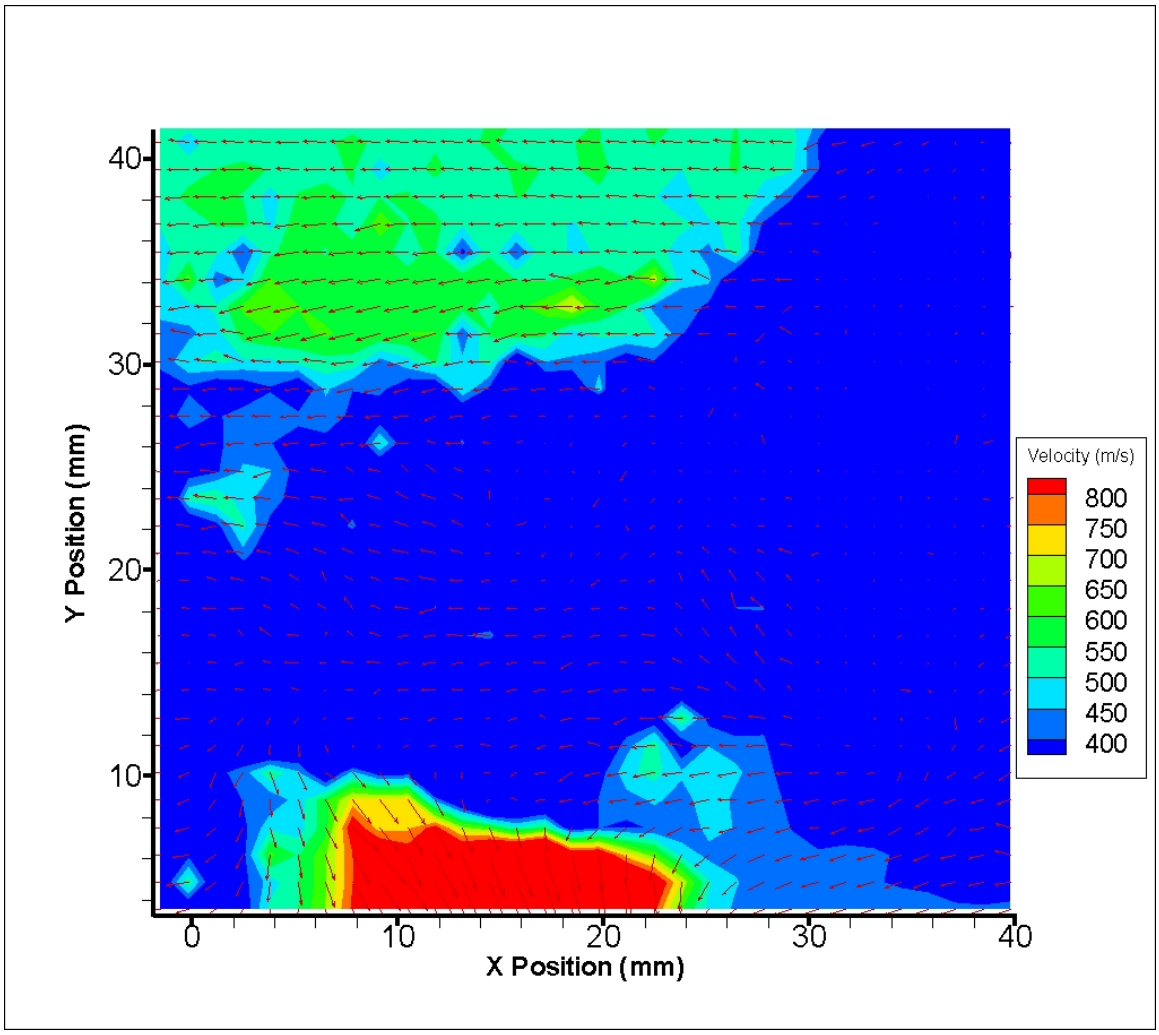

Figure 46: Vector map generated from image pair shown in Figure 44

When the vector map in Figure 46 is compared with the images from Figure 44 and Figure 45, the area of particle seeding quite clearly corresponds to the area of reasonable vectors in the top-left portion of the vector map. The vectors in Figure 46 appear to represent the flow field exactly as expected, with the free stream vectors at the extreme top of the vector map oriented right-to-left with a slightly higher velocity due to the blockage of the model in the test section, and the vectors just aft of the cone

demonstrating a downward turn into the expected low pressure region behind the cone. It is important to note that, since the cone is visible in the images and the particles only fill the top portion of the images, the resulting vector maps contain no meaningful data where the cone is visible or where the particles are not visible in the images.

An additional set of three image pairs from the experimental run conducted with the cone present in the test section is provided in Figure 47, Figure 48 and Figure 49. These images were captured according to the same parameters given in Table 18. An average velocity vector map was generated for the entire set of 42 image pairs generated for this run, which include the image pairs shown in Figure 44 through Figure 49. This average vector map was computed in accordance with the information provided in Chapter three. The top-half of the value-averaged vector map is provided in Figure 50.

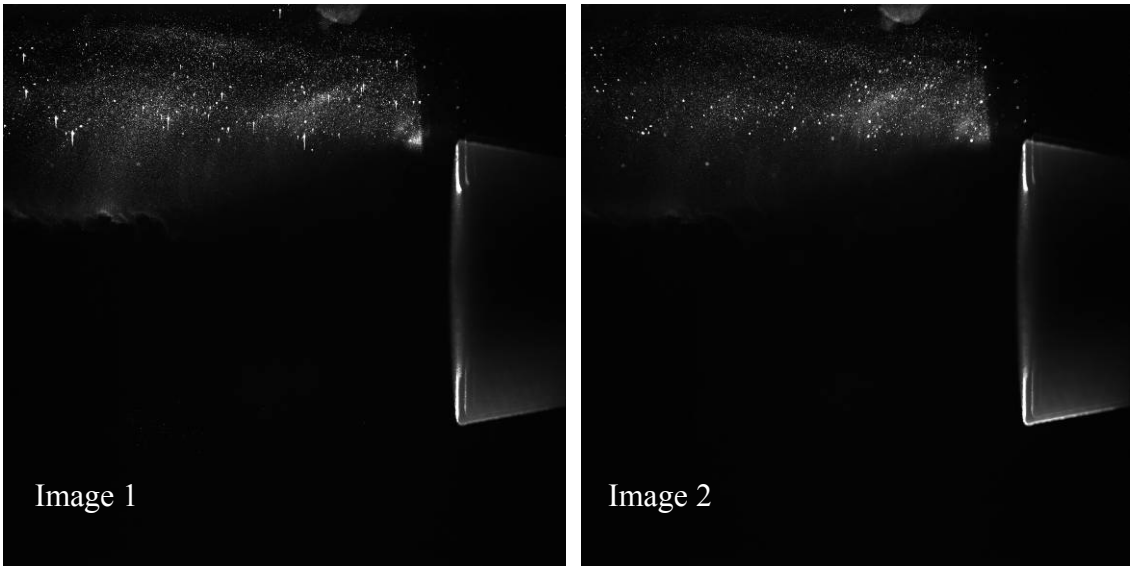

Figure 47: Image pair from shroud injection in nozzle sidewall, with model

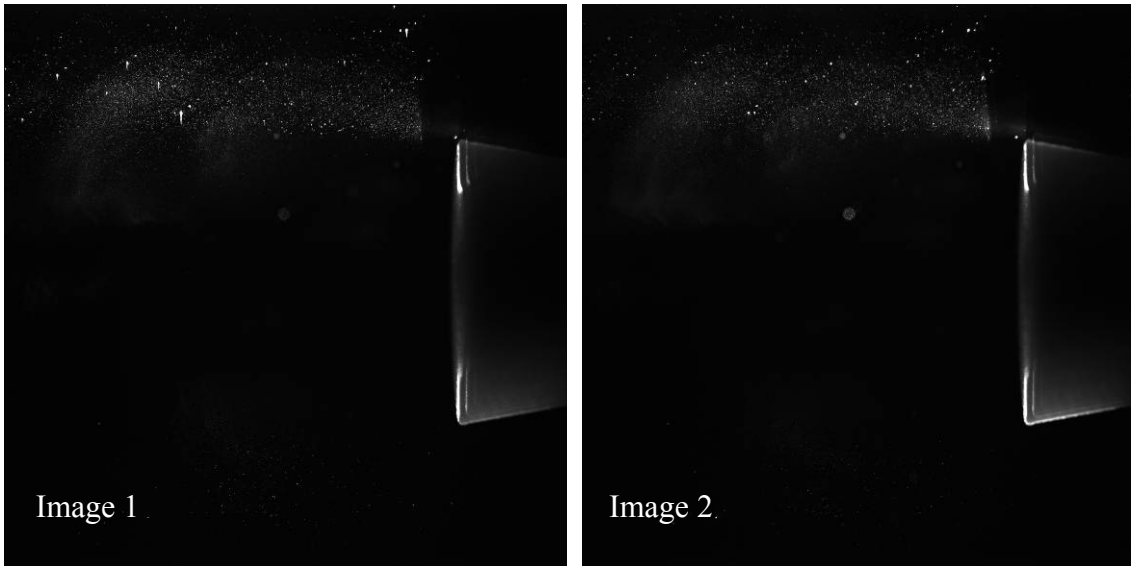

Figure 48: Image pair from shroud injection in nozzle sidewall, with model

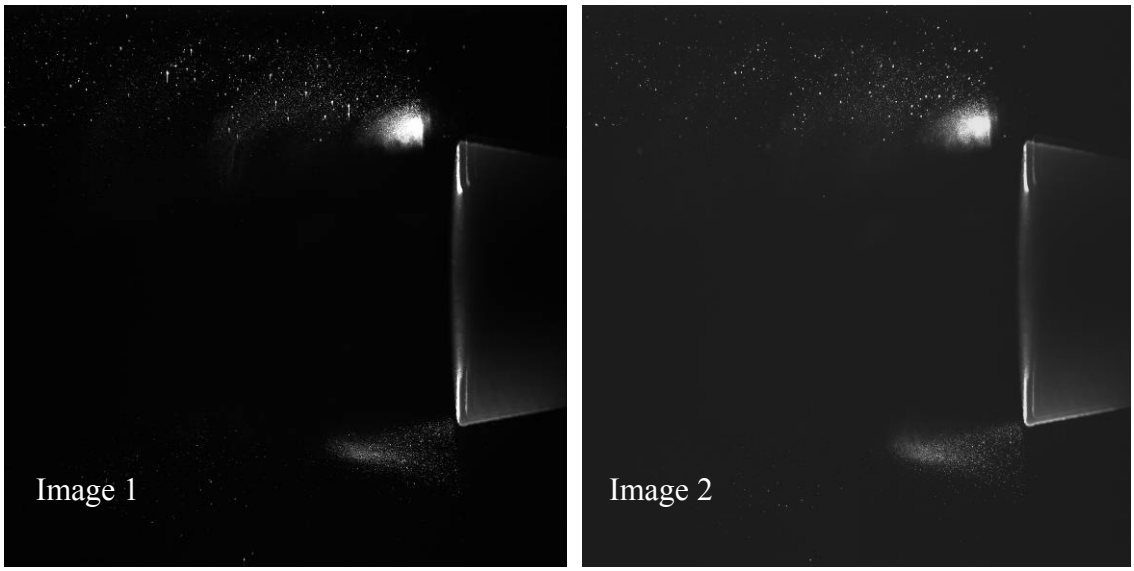

Figure 49: Image pair from shroud injection in nozzle sidewall, with model

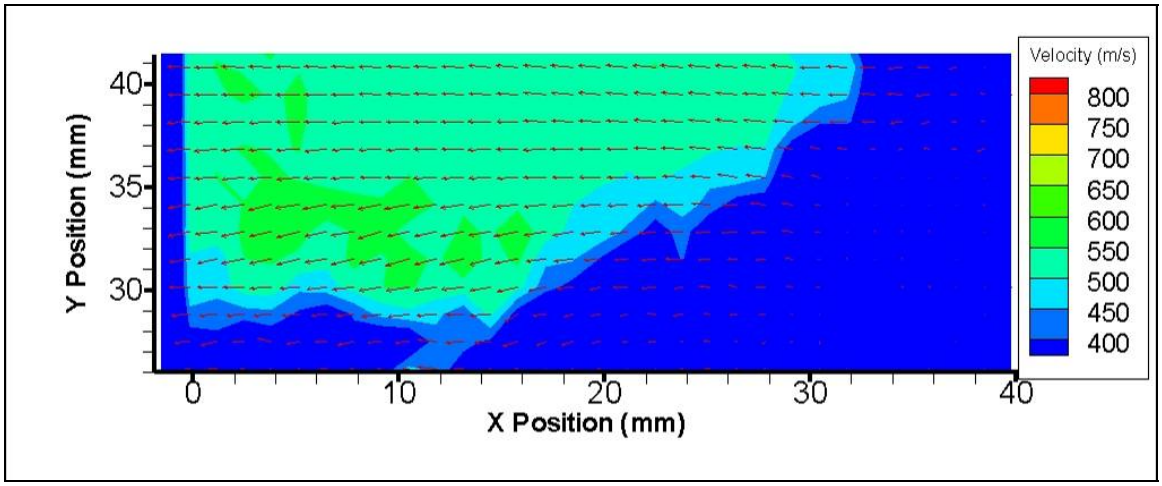

Figure 50: Average vector map (top half) for shroud injection in nozzle sidewall, with model

It was decided to present only the top-half of the average vector map for the experimental run conducted with the cone model in the tunnel because the lower portion of the vector map was not well seeded with CO_2 particles as shown in the image pairs. The flow velocity of approximately 606 m/s is well within the range of velocities calculated in which there was ample particle seeding. In addition, the downward turn in flow direction mentioned earlier in this Chapter is also observed in the average vector map shown in Figure 50.

It can be observed in the average vector map that the areas from the image pairs that do not contain ample particle seeding demonstrate vectors of very low magnitudes. This is a result of the averaging calculation performed on the 42 image pairs in the data set. For each interrogation area that included vectors of very low magnitudes, or directions different from the nominal right-to-left orientation, the contribution for that interrogation to the average vector map was very small or possibly even subtractive. These small vectors are either due to low particle velocities in those interrogation areas or

due to individual image pair vectors that have low magnitudes or directions that cause non-additive or subtractive contributions to the value-averaged vector map.

The ability to generate an average vector map for a large set of image pairs is a valuable tool in the Dantec FlowManager software.

Section 3 – Summary of Results

Upon the generation of the vector map in Figure 46 and others like it, it was determined that vector maps that realistically represented the expected flow field around a portion of the cone model in the test section could be readily produced using the Dantec FlowManager software. This successful demonstration culminated the research effort for this thesis. A summary of all experimental runs conducted during this research is provided in Table 19.

Table 19: Summary of results

Injector Type	Injection Site	Injection Orientation	Results
Multi-port Injector	Converging-diverging nozzle sidewall	Aligned with flow direction	Fog-like particle consistency, severe washout, poor vector maps
		Reverse to flow direction	
		Transverse 90˚ up to flow direction	
	Top of stagnation chamber	Aligned with flow direction	Good particle uniformity through test section, particles too small and fog-like for PIV processing, lighting problems, poor vector maps
		Reverse to flow direction	
Shroud Injector	Top of stagnation chamber	Approximately 2 inches deep in stagnation chamber	Poor particle uniformity through test section, particles too small for PIV processing, lighting problems, poor vector maps
	Converging-diverging nozzle sidewall	Approximately 2 inches deep in nozzle	Mixed fog-like clouds and discrete particles, particle sizes much more conducive to PIV processing, accurate vector maps generated for seeded areas of illumination plane
		Approximately ¾ inch deep in nozzle	Very good vector map accuracy for seeded areas of illumination plane, PIV processing proved possible with model in wind tunnel

V. Conclusions and Recommendations

Section 1 – Conclusions of Research

In conclusion, the use of solid CO_2 particles as a seed material for particle image velocimetry has been successfully demonstrated in a pressure-vacuum closed circuit supersonic wind tunnel of Mach 2.9 nominal velocity and test section area of 2.5 inches by 2.5 inches. Two injector types were investigated at two injection sites relative to the wind tunnel test section. The Dantec FlowManager PIV processing software was successfully manipulated to process images for the generation of vector maps that accurately represented the known flow velocity in the wind tunnel.

The multi-port injector produced fog-like CO_2 particles that were arranged in clouds for each of the three orientations investigated. This particle consistency was not conducive to meaningful vector map generation using the Dantec FlowManager software. When this injector was utilized at the stagnation chamber injection site, the fog-like particle structure was even more evident. The CO_2 particles filled the illumination plane much more fully, creating a very uniform particle density within each image. These particles proved to be too small for effective PIV processing.

An injector using a smaller feed tube releasing CO_2 into a larger shroud tube was utilized at both injection sites as well. When mounted in the stagnation chamber injection site using a 0.030 inch inside diameter feed tube into the 0.19 inch inside diameter shroud tube, the shroud injector produced a very uniform dispersal of small particles that was very similar to the results for the multi-port injector when used at the same injection location. When mounted in the nozzle sidewall, however, the shroud injector produced a mix of fog-like particles and larger discrete particles when utilizing

both the 0.030 inch feed tube and a 0.020 inch feed tube. The preponderance of large discrete CO_2 particles enabled very realistic vector maps to be generated that matched the known flow velocity inside the test section. Upon the insertion of a 10˚ half-angle cone model into the test section, the shroud injector produced particles that enabled successful and realistic PIV processing.

Section 2 – Significance of Research

The use of CO_2 particles as the seed material for PIV represents a great leap forward for flow measurement techniques in closed circuit wind tunnels. The non-intrusiveness of CO_2 particles make this a very valuable injection technique for closed circuit wind tunnels since these particles do not require clean-up or damage wind tunnel components. In addition, the inexpensive nature of compressed liquid CO_2 can make this a much cheaper alternative seeding material for PIV in any type of aerodynamic research. Overall, the use of CO_2 particles for seeding in PIV systems could dramatically reduce operation costs, maintenance costs and wind tunnel down-time due to maintenance and repair while providing results that are just as accurate as those obtained using traditional PIV seeding materials.

Section 3 – Recommendations for Future Research

Having demonstrated the use of CO_2 particle seeding for PIV in an empty test section and with a cone model present in the test section, more research is needed to further refine injection and processing techniques. The design of an injector and feed system that produces consistent properly sized particles of a very uniform nature will require further study. Additionally, more research can be done into the proper location

for injection considering particle residence time in the flow and, thus, particle size and uniformity in the test section.

More research will be required to accomplish these tasks with the presence of various models in the test section as well. The presence of a model in the test section will require the development of an injection technique that enables proper particle sizing and distribution to enable vector generation for all areas of interest around the model. This will also require the development of illumination and imaging techniques that permit the capturing of suitable images for PIV processing.

Appendix

CO_2 to Dry Air Mass Flow Ratio Calculation

An analysis was conducted to determine the mass flow ratio of CO2 to dry air inside the wind tunnel test section. Utilizing the shroud injector in the nozzle sidewall injection site, the liquid CO_2 tank was placed on a digital scale and the run time was measured for an experimental run. The mass flow rate for CO_2 was then calculated using the measured data in Table 20. The CO_2 mass flow rate was calculated using Equation 3.

$$\frac{dm_{CO2}}{dt} = \frac{m_{initial} - m_{final}}{t_{elapsed}} \quad \text{(Eq. 3)}$$

where dm_{CO2}/dt is the mass flow rate of CO_2, $m_{initial}$ and m_{final} are the initial and final masses of the liquid CO2 tank, respectively, and $t_{elapsed}$ is the elapsed time of CO_2 injection during the experiment.

Table 20: Data for CO_2 mass flow rate calculation

Parameter	Measure
Initial mass of tank, $m_{initial}$	60.45 kg
Final mass of tank, m_{final}	60.35 kg
Duration of CO_2 injection, $t_{elapsed}$	15.74 seconds
Calculated CO_2 mass flow rate	6.353×10^{-3} kg/s

After calculating the mass flow rate of CO_2 during particle injection, the mass flow rate of dry air through the wind tunnel was calculated using Equation 4.

$$\frac{dm_{air}}{dt} = \frac{p_o A^*}{\sqrt{T_o}} \sqrt{\left(\frac{\gamma_{air}}{R_{air}}\right)\left(\frac{2}{\gamma_{air}+1}\right)^{\frac{(\gamma_{air}+1)}{(\gamma_{air}-1)}}} \qquad \text{(Eq. 4)}$$

where dm_{air}/dt is the mass flow rate of dry air in the wind tunnel, p_o is the stagnation pressure of the air in the tunnel, A* is the area of the throat of the converging-diverging nozzle, T_o is the stagnation temperature of the air in the tunnel, γ_{air} is the specific heat ratio of air and R_{air} is the gas constant for air. The measured parameters for this calculation and the calculated mass flow rate of dry air are given in Table 21.

Table 21: Data for dry air mass flow rate calculation

Parameter	Measure
Stagnation pressure, p_o	38.4 lb_f/in^2
Stagnation temperature, T_o	293 K
Throat area, A*	1.008×10^{-3} m^2
Gas constant for air, R_{air}	287.1 J/(kg K)
Specific heat ratio for air, γ_{air}	1.4
Calculated mass flow rate of dry air	6.3005×10^{-1} kg/s

Dividing the calculated mass flow rate for CO_2 by the calculated mass flow rate for dry air, the mass flow ratio of CO_2 to dry air was calculated to be 0.01058, or 1.058% CO2 for each unit of dry air. With this very small mass flow ratio for CO_2 and air, it is not believed that the flow regime is being altered dynamically to any appreciable degree.

Calculation of Change in Specific Heat Ratio and Change in Mach Number

Injecting CO_2 into dry air will undoubtedly change the ratio of specific heats for the mixture. This can lead to a change in the Mach number for the flow in the test section, since Mach number is a function of specific heat ratio. To determine the extent to which the specific heat ratio for dry air is being affected by CO_2 injection, a calculation was performed to analyze the specific heat ratio of the mixture. A worst case scenario was analyzed, in which all solid particles have fully sublimated into a gaseous CO_2 state through the nozzle.

Gas properties for CO_2 and air are presented in Table 22 (8). The calculation of the specific heat ratio for the mixture of CO_2 and air was performed according to Equations 5 and 6 assuming uniform mixing and fully sublimated CO_2.

$$\gamma_m = \frac{C_{pm}}{C_{vm}} \qquad \text{(Eq. 5)}$$

where:

$$\frac{C_{pm}}{C_{vm}} = \frac{mf_{CO2} \bullet C_{pCO2} + mf_{air} \bullet C_{pair}}{mf_{CO2} \bullet C_{vCO2} + mf_{air} \bullet C_{vair}} \qquad \text{(Eq. 6)}$$

For Equations 5 and 6, C_{pair}, C_{pCO2} and C_{pm} are the specific heats at constant pressure for air, CO_2 and the mixture, respectively. C_{vair}, C_{vCO2} and C_{vm} are the ratios of specific heats at constant pressure for air, CO_2 and the mixture, respectively In addition, the mass fractions of air and CO_2 are given by mf_{air} and mf_{CO2}. The ratio of specific heats

for the mixture is given by γ_m, and the calculated value and percent reduction from pure air are provided in Table 22.

Table 22: Data for calculation of specific heat ratio for mixture

Parameter	Air	CO_2
Specific heat at constant pressure, C_p	1.007 kJ/(kg K)	0.850 kJ/(kg K)
Specific heat at constant volume, C_v	0.7199 kJ/(kg K)	0.661 kJ/(kg K)
Gas constant, R_{air} and R_{CO2}	0.287 kJ/(kg K)	0.189 kJ/(kg K)
Specific heat ratio, γ_{air} and γ_{CO2}	1.3988	1.2860
Mass fraction of gas, mf	0.01	0.99
Calculated specific heat ratio for mixture, γ_m	1.39777	
Percent reduction in specific heat ratio for mixture versus air	0.0736%	

With a known percent reduction in specific heat ratio for the mixture versus pure dry air, the percent change in Mach number can be calculated using Equations 7 and 8, where a is the speed of sound, M is Mach number, V is velocity, γ is specific heat ratio and T is temperature.

$$a = \sqrt{\gamma RT} \qquad \text{(Eq. 7)}$$

$$M = \frac{V}{a} \qquad \text{(Eq. 8)}$$

For a 0.0736% reduction in specific heat ratio for the mixture versus pure air, the reduction in Mach number for the flow is 0.0488%. This result provides confidence that

CO_2 particle seeding for PIV calculations can be accomplished in this wind tunnel without appreciably altering the Mach number of the flow, allowing the generation of meaningful PIV data.

Bibliography

1. Adrian R.J. "Statistical properties of particle image velocimetry measurements in turbulent flow," *Laser Anemometry in Fluid Mechanics III.* Springer-Verlag: 115-129 (1988).

2. Arnold Engineering Development Center Fact Sheet. http://www.arnold.af.mil/aedc/aerodynamics/index.htm

3. Bjorge, S. et al. "Flow around an object projected from a cavity into a supersonic freestream." *AIAA Journal*. Vol 43, No 7: 1465-1475 (2005)

4. Dantec Dynamics. "Adaptive correlation in FlowManager, Product information." http://www.dantecdynamics.com/Download/litterature/pi_Adaptive_correlation_in_FlowManager33_134.pdf

5. Dantec Dynamics. "FlowManager software and introduction to PIV instrumentation." (2002)

6. DeLapp, C., Reeder, M., Crafton, J. "Clean seeding material for particle image velocimetry measurements." AIAA-2006-2807 (2006).

7. DeLapp, C. "Particle image velocimetry using novel, non-intrusive particle seeding." Masters Thesis, Air Force Institute of Technology (June 2006).

8. Incropera, F., DeWitt, D. *Fundamentals of heat and mass transfer.* 5th printing. Wiley (2001).

9. Jung, T. "Wind Tunnel Study of Interference Effects Relating to Aft Supersonic Ejection of a Store." AFIT Thesis Dec 2005.

10. Keane R.D., Adrian R. J. "Theory of cross-correlation analysis of PIV images." *Applied Science Res.*: 49: 191-215 (1992).

11. Kohlman, D.L. and Richardson, R.W. "Experiments on the Use of Dry Ice Ablating Wind-Tunnel Models." *Journal of Spacecraft and Rockets*, Vol 6, No 9: 1061-1063 (1969).

12. Megerle, M., Sick, V., Reuss, D., "Measurement of digital particle image velocimetry precision using electro-optically created particle image displacements." *Measurements Science Technology.* Vol 13: 997-1005 (2002).

13. Melling A. “Tracer Particles & Seeding for Particle Image Velocimetry.” *Measurement Science Technology*. Vol 8: 1407-1416 (1997).

14. Ming, Q. et al, “Investigation on utilizing laser speckle velocimetry to measure the velocities of nanoparticles in nanofluids.” *Optics Express.* Vol 14, No 17: 7559-7566 (2006)

15. Poggie, J., Erbland, P.J., Smits, A.J., Miles, R.B. “Quantitative visualization of compressible turbulent shear flows using condensate-enhanced Rayleigh scattering.” *Experiments in Fluids.* Vol 37: 438-454 (2004).

16. Raffel, M. Willert, C. Kompenhans J. *Particle Image Velocimetry, A Practical Guide.* 3rd Printing. Springer-Verlag (1998).

17. Rawle, A. “Basic Principles of Particle Sizing,” Malvern Instruments Technical Paper.

18. Scarano F., van Oudheusden, B.W. “PIV investigation of a planar supersonic wake flow”. Delft University of Technology, the Netherlands, paper from: “10th International Symposium of Applications of Laser Techniques to Fluid Mechanics.” http://in3.dem.ist.utl.pt/lxlaser2002/papers/paper_34_1.pdf

19. Willert, C.E., Gharib, M. “Digital Particle Image Velocimetry,” *Experiments in Fluids.* Vol. 10, pp 181-193 (1991).

REPORT DOCUMENTATION PAGE

Form Approved
OMB No. 074-0188

1. REPORT DATE *(DD-MM-YYYY)*	2. REPORT TYPE	3. DATES COVERED *(From – To)*
02-03-2007	Masters Thesis	Sep 2005 – Mar 2007

4. TITLE AND SUBTITLE

Demonstration of clean particle seeding for particle image velocimetry in a closed circuit supersonic wind tunnel

5a. CONTRACT NUMBER

5b. GRANT NUMBER

5c. PROGRAM ELEMENT NUMBER

6. AUTHOR(S)

McNiel, Charles M., 1Lt, USAF

5d. PROJECT NUMBER
JON ENY06-382

5e. TASK NUMBER

5f. WORK UNIT NUMBER

7. PERFORMING ORGANIZATION NAMES(S) AND ADDRESS(S)
Air Force Institute of Technology
Graduate School of Engineering and Management (AFIT/EN)
2950 Hobson Way, Building 640
WPAFB OH 45433-8865

8. PERFORMING ORGANIZATION REPORT NUMBER
AFIT/GAE/ENY/07-M19

9. SPONSORING/MONITORING AGENCY NAME(S) AND ADDRESS(ES)
Julie Saladin
AFRL/VAAI
WPAFB OH 45433

10. SPONSOR/MONITOR'S ACRONYM(S)

11. SPONSOR/MONITOR'S REPORT NUMBER(S)

12. DISTRIBUTION/AVAILABILITY STATEMENT

APPROVED FOR PUBLIC RELEASE; DISTRIBUTION UNLIMITED.

13. SUPPLEMENTARY NOTES

14. ABSTRACT

The purpose of this research was to determine whether solid carbon dioxide (CO_2) particles might provide a satisfactory, and cleaner, alternative to traditional seed material for Particle Image Velocimetry (PIV) for use in a closed circuit supersonic wind tunnel. The Air Force Institute of Technology (AFIT) closed circuit pressure-vacuum supersonic wind tunnel was utilized, which achieves a nominal Mach number of Mach 2.9 in a 2.5 inch by 2.5 inch square test section. CO_2 was dispensed into the flow as a liquid from a standard compressed gas liquid tank through two different injector styles at two injection sites using various injector attitudes. Upon exiting the injector in either the stagnation chamber or converging-diverging nozzle, the liquid CO_2 rapidly formed solid particles which became entrained in the wind tunnel flow and began the sublimation process from a solid to a gaseous state. The particles traveled through the test section, in which they were illuminated by a laser, and the light scattered by the particles was imaged with a camera. The resulting images were processed using the Dantec Dynamics FlowManager PIV processing software to generate vector maps representing the flow field in the test section. The particles fully sublimated after traveling through the test section, making the injection process self cleaning and hazard free. Vector maps that matched the nominal 606 m/s velocity in the empty test section were generated utilizing both multi-port tube and shroud tube style injectors. Realistic vector maps were also generated for the flow with a 10˚ half-angle cone model placed inside the test section. Overall this research successfully demonstrated the use of CO_2 as a seed material for PIV processing.

15. SUBJECT TERMS

Particle Image Velocimetry, Seed Particles, Tracer Particles, Carbon Dioxide

16. SECURITY CLASSIFICATION OF:			17. LIMITATION OF ABSTRACT	18. NUMBER OF PAGES	19a. NAME OF RESPONSIBLE PERSON
a. REPORT	b. ABSTRACT	c. THIS PAGE			Mark F. Reeder
U	U	U	UU	111	19b. TELEPHONE NUMBER *(Include area code)* (937) 255-6565, ext 4530 (mark.reeder@afit.edu)